polyvinylidene difluoride membrane (Immobilon-P; Millipore, Bedford, MA, USA) as previously described (Shimazawa *et al.* 2007a). The primary antibodies used were as follows: rabbit anti-NR1 (ImmuQuest, Cleveland, UK), anti-NR2B (R&D Systems Inc., Minneapolis, MN, USA), mouse anti-human APP (6E10; Covance, Emeryville, CA, USA), rabbit anti-phospho-calcium/calmodulin-dependent protein kinase IIα (p-CaMKIIα; Santa Cruz, Santa Cruz, CA, USA), rabbit anti-CaMKII (Santa Cruz), and mouse anti-β-actin (Sigma–Aldrich).

Immunostainings

At various times after intravitreal injection, eyes were enucleated, fixed in 4% paraformaldehyde overnight at 4°C, immersed in 20% sucrose for 48 h at 4°C, and finally embedded in optimum cutting-temperature compound. Transverse, 10-μm-thick cryostat sections or 4-μm-thick paraffin-embedded sections, which prepared as described in Histological analysis, were cut and subsequently processed for immunohistochemical or immunofluorescent staining using the appropriate antibody against $A\beta_{1-42}$ (1 : 1000 dilution in PBS; FCA3542; Calbiochem), NR1 (1 : 400; ImmuQuest) or p-CaMKIIα (1 : 50; Santa Cruz) as described in our previous reports (Suemori *et al.* 2006; Shimazawa *et al.* 2007a). For $A\beta_{1-42}$ immunostaining, the frozen sections were treated with 90% formic acid for 5 min at 25°C, 0.05% tyrosine solution for 15 min at 37°C, and MOM blocking solution (Vector, Burlingame, CA, USA) for 30 min at 25°C before incubation with the primary antibody for overnight at 4°C. After incubation with each primary antibody, the sections were incubated either (a) with Alexa Fluor-488-conjugated secondary antibody (1 : 2000 dilution in PBS; Molecular Probes, Eugene, OR, USA) for 1 h at 25°C, mounted with a coverslip, and observed under an epifluorescence microscopy (Power BX50; OLYMPUS, Tokyo, Japan), or (b) with biotin-conjugated secondary antibody for 1 h at 25°C, and visualized using a VECTOR M.O.M. Immunodetection kit (Vector).

Terminal deoxynucleotidyl transferase–mediated dUTP nick end-labeling (TUNEL) staining

Twenty-four hours after intravitreal injection of NMDA, eyes were enucleated, fixed in 4% paraformaldehyde overnight at 4°C, immersed in 20% sucrose for 48 h at 4°C, and finally embedded in optimum cutting-temperature compound. Transverse, 10-μm-thick cryostat sections were cut and subsequently processed for TUNEL staining. TUNEL assay was performed using an *in situ* cell death detection kit, POD (Cat. No. 11 684 817 910, Roche Molecular Biochemicals Inc., Mannheim, Germany) according to the manufacturer's instructions. Light-microscope images were photographed, and the TUNEL-positive cells in the ganglion cell layer (GCL) at a distance between 350 and 750 μm from the optic disc were measured on the photographs in a masked fashion by a single observer (M.S.).

Photopic electroretinogram recording

For electroretinogram (ERG) recording, the right eye was stimulated (with the pupil fully dilated using 0.4% tropicamide), while the left eye was carefully patched to avoid stray-light stimulation. The ERG response was recorded on a computer, where they were digitized and stored for analysis (MacLab 2e; AD Instruments, Castle Hill, Australia). In these experiments, mice were anesthetized with an intraperitoneal injection of xylazine (0.05 mg/g body weight) plus ketamine (0.1 mg/g body weight).

The photopic negative response (PhNR), which follows the b-wave, has been shown to originate from the inner retinal neurons (Viswanathan *et al.* 2000, 2001). PhNR was recorded with a light emitting diode (LED) built-in a contact lens electrode (model LS-C; Mayo Corporation, Inazawa, Japan). After 15 min of light adaptation, a PhNR was elicited by a white stimulus of 35.4 cd·s/m^2 on a white background of 39.8 cd/m^2. The PhNR amplitude was measured from the baseline to the negative trough between the cone b-waves and i-waves.

Statistical analysis

Data are presented as the means ± SEM. Statistical comparisons were made using a Student's *t*-test, Dunnett's test, or Tukey–Kramer test, with $p < 0.05$ being considered to indicate statistical significance.

Results

Concentrations of $A\beta_{1-40}$ and $A\beta_{1-42}$ in soluble or insoluble fraction of forebrain and retinal extracts

To explain Aβ accumulation in the forebrains of APP transgenic (Tg) mice (Tg 2576), mutant presenilin-1 (PS-1) knock-in mice, APP/PS-1 double Tg mice, and wild-type mice at age 11 or 24 months, the concentrations of $A\beta_{1-40}$ and $A\beta_{1-42}$ in 1% Triton X-100 (Tx)-soluble (defined as soluble Aβ) and -insoluble (defined as insoluble Aβ) fractions were measured using human specific $A\beta_{1-40}$ or $A\beta_{1-42}$ ELISA kit (BioSource International Inc., Camarillo, CA, USA), as shown in Fig. S1a–d. In the PS-1 knock-in mouse forebrain, there were no significant differences in either the soluble or insoluble forms of $A\beta_{1-40}$ and $A\beta_{1-42}$ at 24-months versus the wild-type mouse brain. In the APP Tg mouse forebrain, the soluble and insoluble forms of $A\beta_{1-40}$ and $A\beta_{1-42}$ were increased at 24 months. In the APP/PS-1 Tg mouse forebrain, the soluble and insoluble forms of $A\beta_{1-40}$ and $A\beta_{1-42}$ were increased at 11 months, and they were further increased at 24 months.

To examine Aβ accumulation in the retinas of PS-1 knock-in mice, APP/PS-1 double Tg mice, and wild-type mice at 11- or 24-months old, the concentrations of $A\beta_{1-40}$ in the 0.2% DEA-soluble (defined as soluble Aβ) and -insoluble (defined as insoluble Aβ) fractions were measured using high-sensitivity human $A\beta_{1-40}$ ELISA kit (Immuno-Biological Laboratories Co., Ltd.), as shown in Fig. 1a and b. In the wild-type mouse retina: the soluble $A\beta_{1-40}$ concentration was 6.75 ± 1.23 pmol/mg protein ($n = 8$) at 11 months and 9.60 ± 2.34 pmol/mg protein ($n = 4$) at 24 months, while the insoluble $A\beta_{1-40}$ concentration was 20.35 ± 5.17 pmol/mg protein ($n = 8$) at 11 months and 31.09 ± 7.34 pmol/mg protein ($n = 4$) at 24 months. In the PS-1 knock-in mouse retina, there was no significant difference in either the soluble

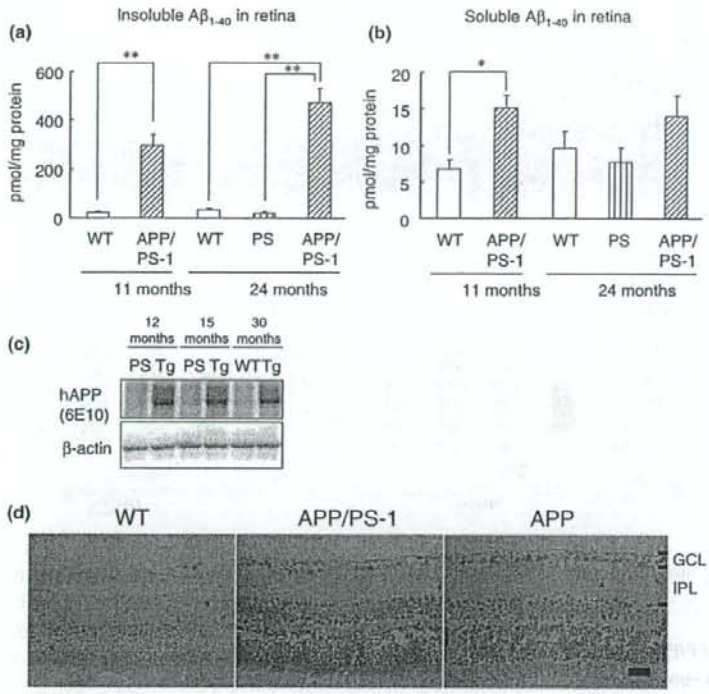

Fig. 1 Amyloid-β (Aβ) and amyloid precursor protein (APP) accumulations in retinas of human mutant APP transgenic (Tg) mice (Tg 2576), mutant presenilin-1 (PS-1) knock-in mice, APP/PS-1 double Tg mice, and wild-type mice. (a) Insoluble $A\beta_{1-40}$ in retina. (b) Soluble $A\beta_{1-40}$ in retina. Each column represents the mean ± SEM ($n = 3$–8). *, $p < 0.05$; **, $p < 0.01$ (Tukey–Kramer test). 11M, 11-month-old, 24M, 24-month-old. WT, wild-type mouse. PS, PS-1 knock-in mouse. (c) Immunoblots for human APP detected with anti-APP antibody (6E10). 12M, 12-month-old, 15M, 15-month-old, 30M, 30-month-old. Tg, APP/PS-1 double Tg mouse. (d) Immunohistochemistry for $A\beta_{1-42}$. Scale bar: 25 μm.

or insoluble form of $A\beta_{1-40}$ at 24-months old versus the wild-type mouse retina. In the APP/PS-1 Tg mouse retina, both soluble and insoluble $A\beta_{1-40}$ were increased to 20.4 ± 5.2 pmol/mg protein ($n = 8$) and to 294.2 ± 47.2 pmol/mg protein ($n = 6$), respectively) at 11 months, and insoluble $A\beta_{1-40}$ was significantly increased to 472.9 ± 59.8 pmol/mg protein ($n = 3$) at 24 months [soluble $A\beta_{1-40}$ tended to be increased (1.4-fold) at 24 months but significance was not established].

$A\beta_{42}$ and APP accumulations in mouse retinas

In the APP/PS-1Tg mouse retina, mutated human APP protein was detected using a human APP specific antibody (6E10) (Fig. 1c). In the APP/PS-1 Tg mouse retina, human APP protein was expressed at 12-, 15- and 30-months, and their increased levels were similar among these ages. On the other hand, there was no detectable APP protein in wild-type mouse retina (30-months old) or mutant presenilin-1 (PS-1) knock-in mouse retina (12- or 15-months old). When we immunohistochemically evaluated the accumulation of $A\beta_{1-42}$ in the retina using an $A\beta_{1-42}$-specific antibody (FCA3542) (Fig. 1d), $A\beta_{1-42}$ immunoreactivity was found to be increased in the cells of the GCL, inner nuclear layer, and outer nuclear layer in APP Tg and APP/PS-1 Tg mouse retinas (24-months old) contrary to our prediction: $A\beta_{1-42}$ is known to accumulate and form amyloid plaques in the Alzheimer's brain. On the other hand, there was no immunoreactivity in the wild-type mouse retina at 24-months old.

Histological comparisons of non-treated retinas among APP Tg mice, PS-1 knock-in mice, APP/PS-1 double Tg mice, and wild-type mice

Histological changes were examined in the non-treated retinas of 12-month-old APP Tg mice, PS-1 knock-in mice, APP/PS-1 double Tg mice versus wild-type mice (Fig. S2a shows representative photographs). There were no significant differences in GCL cell numbers (Fig. S2b) or inner plexiform layer (IPL) thickness (Fig. S2c) between all Tg mouse groups and wild-type mice.

Comparison among APP Tg mice, PS-1 knock-in mice, APP/PS-1 double Tg mice, and wild-type mice regarding NMDA-induced retinal damage

The retinal damage induced by NMDA was compared between 15-month-old Tg mice and wild-type mice at 7 days after NMDA injection (Fig. 2a shows representative photographs). Morphometric changes in GCL cell number (Fig. 2b) and IPL thickness (Fig. 2c) were quantified from retinal cross-sections. In wild-type mice, intravitreal injection of NMDA at 5 nmol/eye significantly decreased both the GCL cell number and the IPL thickness (vs. non-treated control eyes). APP Tg and APP/PS-1 Tg mice, but not PS-1 Tg mice, displayed less retinal damage (decreases

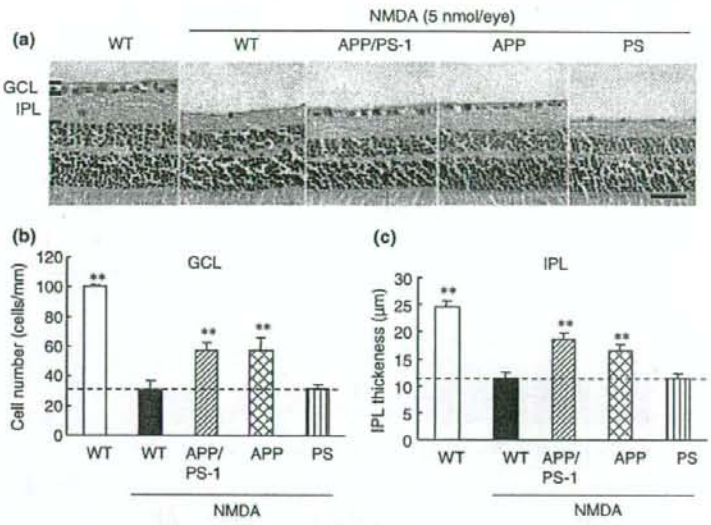

Fig. 2 Comparison of NMDA-induced retinal damage among three types of transgenic mice and wild-type mice. (a) Representative photographs showing retinas obtained from human mutant amyloid precursor protein (APP) transgenic (Tg) mice (Tg 2576), mutant presenilin-1 (PS-1) knock-in mice, APP/PS-1 double Tg mice, and wild-type mice at 7 days after NMDA injection. NMDA at 5 nmol/eye was administered into the intravitreal space. Scale bar: 25 μm. Quantitative analysis of cell number in ganglion cell layer (GCL) (b) and inner plexiform layer (IPL) thickness (c). Each column represents the mean ± SEM ($n = 8$–10). **, $p < 0.01$ versus NMDA-treated in wild-type mice (Tukey–Kramer test).

in GCL cell number and IPL thickness) than wild-type mice.

Comparison between PS-1 knock-in and APP/PS-1 double Tg mouse retinas on the increase of TUNEL-positive cells after NMDA injection

The TUNEL-positive cells induced by NMDA was compared between 15-month-old APP/PS-1 double Tg mice and PS-1 knock-in mice at 24 h after NMDA injection (Fig. 3a, arrows), and the number of TUNEL-positive cells in GCL was quantified from retinal cross-sections (Fig. 3b). In non-treated retinas of both APP/PS-1 double Tg and PS-1 knock-in mice, few TUNEL-positive cells were observed in GCL. In PS-1 knock-in mice, intravitreal injection of NMDA at 5 nmol/eye significantly increased TUNEL-positive cells in both the GCL (vs. non-treated control eyes). APP/PS-1 double Tg mice significantly displayed less number of TUNEL-positive cells in GCL than PS-1 knock-in mice.

Effect of DAPT, a γ-secretase inhibitor, on *N*-methyl-D-aspartate (NMDA)-induced retinal damage in PS-1 knock-in and APP/PS-1 double Tg mice

The effect of DAPT on the retinal damage induced by NMDA was compared between 15-month-old PS-1 knock-in and APP/PS-1 double Tg mice at 7 days after NMDA

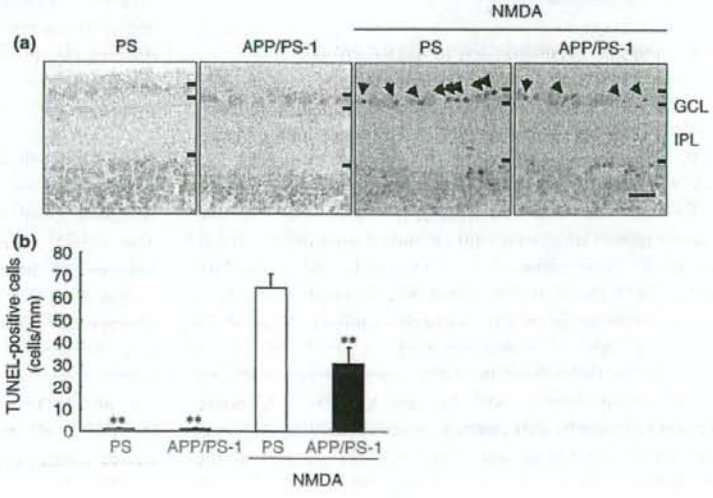

Fig. 3 Comparison between retinas of mutant presenilin-1 (PS-1) knock-in and human mutant amyloid precursor protein (APP) and PS-1 (APP/PS-1) double transgenic (Tg) mice on TUNEL-imunostainings at 24 h after NMDA injection. (a) Representative photographs showing retinas obtained from PS-1 knock-in mice and APP/PS-1 double Tg mice at 24 h after NMDA injection. NMDA at 5 nmol/eye was administered into the intravitreal space. Scale bar: 20 μm. Arrows show TUNEL-positive cells in ganglion cell layer (GCL). IPL, inner plexiform layer. (b) Quantitative analysis of TUNEL-positive cell number in GCL. Each column represents the mean ± SEM ($n = 8$–10). **, $p < 0.01$ versus NMDA-treated in PS-1 knock-in mice (Tukey–Kramer test).

Table 1 Effect of DAPT, a γ-secretase inhibitor, on *N*-methyl-D-aspartate (NMDA)-induced retinal damage of human mutant amyloid precursor protein (APP) and mutant presenilin-1 (PS-1) double transgenic (APP/PS-1 Tg) mice and PS-1 knock-in mice

Mice	Drug	Treatment	Cell number in GCL (cells/mm)	IPL thickness (μm)
PS-1	Vehicle	–	89.7 ± 2.9**	30.0 ± 0.4**
PS-1	Vehicle	NMDA	29.2 ± 4.9	17.2 ± 1.2
PS-1	DAPT	NMDA	29.1 ± 2.0	16.3 ± 0.7
APP/PS-1	Vehicle	NMDA	49.1 ± 7.3**	23.3 ± 1.5**
APP/PS-1	DAPT	NMDA	25.9 ± 2.6##	15.4 ± 0.7##

Data represent the mean ± SEM ($n = 8$). NMDA at 5 nmol/eye was administered into the intravitreal space. DAPT (100 mg/kg) or vehicle (10 mL/kg) was subcutaneously administered 3 h before and just after NMDA injection. Scale bar: 25 μm. Quantitative analysis of cell number in ganglion cell layer (GCL) and inner plexiform layer (IPL) thickness. **, $p < 0.01$ versus vehicle plus NMDA-treated PS-1 knock-in mice; ##, $p < 0.01$ versus vehicle plus NMDA-treated APP/PS-1 mice (Tukey–Kramer test).

injection (Table 1). In vehicle-treated PS-1 knock-in mice, intravitreal injection of NMDA at 5 nmol/eye significantly decreased both the GCL cell number and the IPL thickness (vs. non-treated control eyes). Vehicle-treated APP/PS-1 Tg mice displayed less retinal damage (decreases in GCL cell number and IPL thickness) than PS-1 knock-in mice. Treatment with DAPT at 100 mg/kg s.c. (3 h before and just after NMDA) significantly diminished the reduced damages in APP/PS-1 Tg mice. On the other hand, there were no significant differences in the retinal damages of PS-1 knock-in mice between DAPT and vehicle treatments.

Retinal expression and localization of NMDA receptor 1 (NR1) in PS-1 knock-in, APP Tg, APP/PS-1 double Tg, and wild-type mice

To clarify the mechanisms underlying the reduced retinal damage observed in APP and APP/PS-1 double Tg mice, the expression and localization of NR1 in the retina were measured using western blotting and immunostaining. Representative band images show immunoreactivities against NR1 and β-actin (Fig. 4a), and the band densities were quantitatively analyzed (Fig. 4b). There was no significant difference in NR1 protein expression between APP/PS-1 Tg and wild-type mouse retinas. As shown in Fig. 4(c–e), localization of NR1 protein in the retina was evaluated using immunofluorescence staining. In the PS-1 knock-in mouse retina (used as a control), NR1 protein was distributed in GCL and IPL, and condensed localizations were seen within cell bodies in GCL (Fig. 4c, arrows). On the other hand, no such localizations could be seen within GCL cell bodies in APP/PS-1 or APP mice (Fig. 4d and e). In our preliminary examination, there was little difference in the distribution of NR1 protein between the wild-type and PS-1 knock-in mouse retina.

Phosphorylated form of calcium/calmodulin-dependent protein kinase IIα (p-CaMKIIα) and total CaMKIIα in non-treated retinas of PS-1 knock-in, APP Tg, APP/PS-1 double Tg, and wild-type mice

CaMKIIα is known to be a key molecule regulating cellular physiological functions, such as long-term potentiation after NMDA-receptor activation (Merrill *et al.* 2005). The immunohistochemical images in Fig. 5(a) show the expression and distribution of the phosphorylated form of CaMKIIα (p-CaMKIIα) in the non-treated retinas of PS-1 knock-in, APP and APP/PS-1 Tg mice. In the PS-1 knock-in mouse retina (used as a control), p-CaMKIIα-like immunoreactivity was detected within cells in GCL (arrows). Compared with these levels, less p-CaMKIIα-like immunoreactivity was detected within GCL cells in APP/PS-1 and APP Tg mice. In our preliminary examination, there was little difference in the distribution of p-CaMKIIα-like immunoreactivity between the wild-type and PS-1 knock-in mouse retina. To compare the p-CaMKIIα level between wild-type and APP/PS-1 mouse retinas, p-CaMKIIα and total CaMKIIα proteins in retinal extracts were detected using an immunoblotting technique, and the band intensities were quantified (Fig. 5b and c). The p-CaMKIIα protein was significantly decreased in APP/PS-1 mice versus wild-type mice, although there was no difference in total CaMKIIα protein between these mice. CaMKIIα is translocated from the cytosolic fraction to the membrane fraction following binding to NMDA-receptor subunits (NR1 and NR2B) and its phosphorylation (Colbran 2004). The CaMKIIα in the retinal membrane fraction was significantly decreased in APP/PS-1 mice versus wild-type mice (Fig. 5d and e). Although there was no difference in NR1 protein in the retinal membrane fraction between these mice, NR2B protein in retinal membrane fraction was significantly decreased in APP/PS-1 Tg mice as compared with wild-type mice (Fig. 5d and f).

Phosphorylated form of CaMKIIα and total CaMKIIα in NMDA-treated retinas of APP/PS-1 double Tg and wild-type mice

In the wild-type mouse retina, p-CaMKIIα, but not total CaMKIIα, was markedly increased (four-fold vs. non-treated mice) at 30 min after NMDA injection at 2 nmol/eye (Fig. S3a and b). The NMDA-induced increase in retinal p-CaMKIIα in the APP/PS-1 was about 60% of that in the wild-type mouse.

Retinal function in APP/PS-1 double Tg mice and wild-type mice as revealed using electroretinogram recordings

To evaluate retinal function, scotopic and photopic ERGs were recorded in APP/PS-1 double Tg mice and

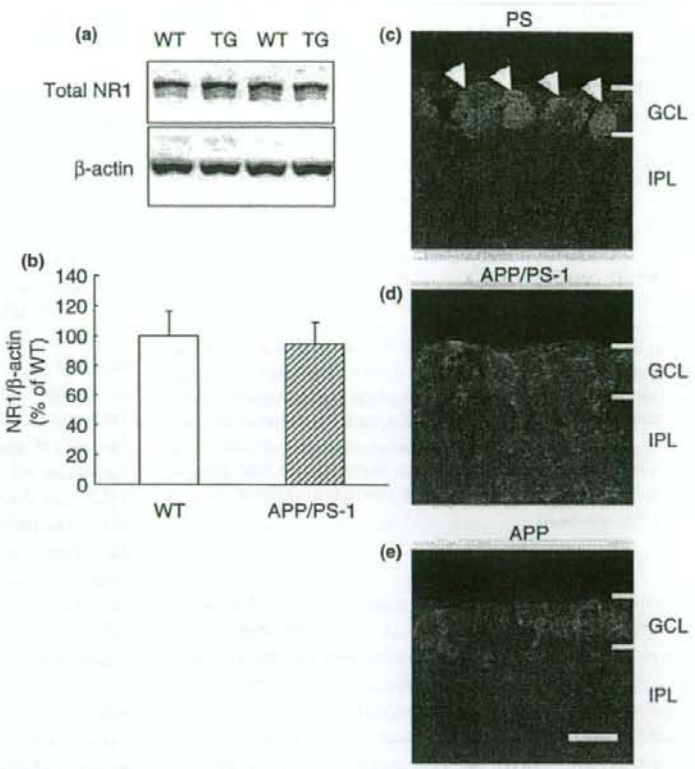

Fig. 4 Expression and localization of *N*-methyl-D-aspartate (NMDA) receptor 1 (NR1) in retinas of human mutant amyloid precursor protein (APP) transgenic (Tg) mice (Tg 2576), mutant presenilin-1 (PS-1) knock-in mice, APP/PS-1 double Tg mice, and wild-type mice. (a) Representative band images show immunoreactivity against NR1. WT, wild-type mice; TG, APP/PS-1 double Tg mice. (b) Quantitative analysis of band densities for NR1. Data are expressed as mean ± SEM ($n = 6$) of values (in arbitrary units) obtained from each band. Localization of NR1 protein in retinal cross-sections from PS-1 knock-in (c), APP/PS-1 double Tg mice (d) or APP Tg mice (e). PS, PS-1 knock-in mice. Arrows show cell bodies in ganglion cell layer (GCL). IPL, inner plexiform layer. Scale bar: 10 μm.

wild-type mice. Fig. S4 shows representative scotopic ERG recordings (Fig. S4a) and the quantitative results obtained for the a-wave (Fig. S4b) and the third oscillation potential (OP-3) (Fig. S4c). In APP/PS-1 Tg mice, both latencies (a-wave and OP-3) were significantly prolonged versus those in wild-type mice. On the other hand, there was no significant difference in either a-wave or OP-3 amplitude between these mice (data not shown). In APP/PS-1 Tg mice, amplitude of photopic negative response (PhNR) and ratio of PhNR to b-wave, but not b-wave, was significantly reduced than those in wild-type mice (Table 2).

Visual function in APP/PS-1 double Tg mice and wild-type mice as revealed using visual-evoked potential recordings

To evaluate visual function, scotopic visual-evoked potentials (VEPs) were recorded in APP/PS-1 double Tg mice and wild-type mice. Figure S5 shows representative VEP recordings (Fig. S5a) and the quantitative results for P1 (Fig. S5b) and N1 (Fig. S5c). In APP/PS-1 Tg mice, both latencies (P1 and N1) were significantly prolonged versus those in wild-type mice. On the other hand, there was no significant difference in P1-N1 amplitude between these mice (data not shown).

Discussion

The present study was performed to assess the functional roles played by Aβ and APP in retinal damage and retinal function, using transgenic mice in vivo [human mutant APP transgenic (Tg) mice (Tg2576), mutant PS-1 knock-in mice, and their double Tg counterparts (APP/PS-1 Tg mice)].

To elucidate the role performed by Aβ in the retina, we used three types of transgenic mice. The APP Tg mouse (Tg2576) carries a transgene (coding for the 695 amino acid isoform of human APP) derived from a large Swedish family with early-onset Alzheimer's disease (Hsiao *et al.* 1996). This mouse expresses a high concentration of mutant Aβ, forms amyloid plaques, and displays memory deficits at 9- to 10-months old. In the present study, APP Tg mice exhibited increases in soluble and insoluble $A\beta_{1-40/1-42}$ in forebrain extracts at 24-months old. On the other hand, the PS-1 knock-in mouse carries a transgene derived from a Japanese family with familial Alzheimer's disease caused by the I213T mutation of PS-1 (Nakano *et al.* 1999). This mouse's mutated PS-1 can cleave APP to $A\beta_{1-42(43)}$ peptide, rather than to $A\beta_{1-40}$ peptide. It exhibits a higher concentration of $A\beta_{1-42}$ than of $A\beta_{1-40}$ at 4–5 months of age, but shows no memory defects. The APP/PS-1 double Tg mouse, which

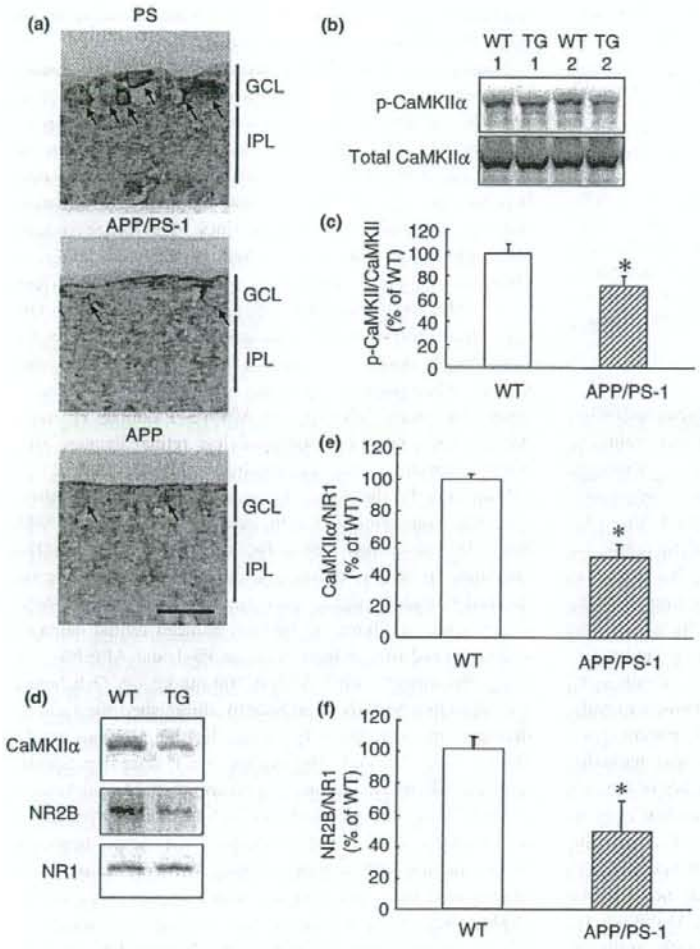

Fig. 5 Phosphorylated form of calcium/calmodulin-dependent protein kinase IIα (p-CaMKIIα) and total CaMKIIα in retinas of human mutant amyloid precursor protein (APP) transgenic (Tg) mice (Tg 2576), mutant presenilin-1 (PS-1) knock-in mice, APP/PS-1 double Tg mice, and wild-type mice. (a) Representative immunohistochemical images show immunoreactivity against p-CaMKIIα in retinal cross-sections. PS, PS-1 knock-in mice; APP, APP Tg mice; APP/PS-1, APP/PS-1 double Tg mice. Scale bar: 10 μm. GCL, ganglion cell layer; IPL, inner plexiform layer. (b) Representative band images show immunoreactivities against p-CaMKIIα and total CaMKIIα in retinal extracts. WT, wild-type mice; TG, APP/PS-1 double Tg mice. (c) Quantitative analysis of band densities for p-CaMKIIα against CaMKIIα in retinal extracts. Data are expressed as mean ± SEM ($n = 4$) of values (in arbitrary units) obtained from each band. *, $p < 0.05$ versus wild-type mouse retina (Student's *t*-test). (d) Representative band images of CaMKII, NR2B and NR1 in membrane fraction of retina. (e) Quantitative analysis of band densities for CaMKIIα and NR2B against NR1 in membrane fraction of retina. Data are expressed as mean ± SEM ($n = 4$) of values (% of WT) obtained from each band. *, $p < 0.05$ versus wild-type mouse retina (Student's *t*-test).

was generated by crossbreeding these two lines, exhibits severe memory defects at 3 months, and $A\beta_{1-40}$ and $A\beta_{1-42}$ deposits are present within the brain at 8 months of age [earlier than in APP Tg mice, which show them at 12 months of age (unpublished data)]. In our study, APP/PS-1 double Tg mice exhibited increased levels of soluble and insoluble $A\beta_{1-40/1-42}$ in forebrain extracts at both 11- and 24-months old. Our findings therefore demonstrate that both APP Tg and APP/PS-1 double Tg mice show increased $A\beta_{1-40/1-42}$ levels in the forebrain, with APP/PS-1 double Tg mice having greater accumulations of $A\beta_{1-40/1-42}$ than APP Tg mice.

Next, we looked for accumulations of APP and Aβ in the retina in these animal models of Alzheimer's disease. Mutated human APP was markedly increased in retinal extracts from APP/PS-1 double Tg mice at 12-,15-, and 30-months old (vs. age-matched wild-type or PS-1 knock-in mice), and their increased levels were similar among these ages. On the other hand, there was no detectable human APP in PS-1 knock-in mouse retina (12- and 15-months old) or wild-type mouse retina (30-months old). Furthermore, (a) in APP/PS-1 mouse retinas, both soluble and insoluble $A\beta_{1-40}$ were increased at 11- and 24-months old, but (b) there was no change in soluble or insoluble $A\beta_{1-40}$ in PS-1 knock-in mouse retinas (vs. age-matched wild-type mice). In this study for the measurement of $A\beta_{1-40}$ in retina, we used other high-sensitivity human $A\beta_{1-40}$ ELISA kit (Immuno-Biological Laboratories Co., Ltd.), because retinal sample needed higher sensitivity than brain. Although this ELISA has approximately six-fold higher sensitivity than BioSource ELISA measured brain $A\beta_{1-40}$, it shows 10–40% cross-reactivity with rodent $A\beta_{1-40}$. On the other hand, BioSource $A\beta_{1-40}$ ELISA is specific for human without rodent $A\beta_{1-40}$ (approximately 0.5% cross-reactivity with rodent $A\beta_{1-40}$).

Table 2 Amplitudes of photopic negative response (PhNR) and b-wave in APP/SP-1 double transgenic and wild-type mice

	PhNR (×100 μV)	PhNR/b-wave	b-wave (×100 μV)
WT	0.51 ± 0.07	0.28 ± 0.03	1.86 ± 0.20
APP/PS-1	0.17 ± 0.07*	0.12 ± 0.03*	1.32 ± 0.29

Data represent the mean ± SEM ($n = 4$). WT: wild-type mice, APP/PS-1: APP/PS-1 Tg mice. *, $p < 0.05$ versus WT (Student *t*-test). PhNR was recorded with a light emitting diode built-in a contact lens electrode. After 15 min of light adaptation, a PhNR was elicited by a white stimulus of 35.4 cd s/m^2 on a white background of 39.8 cd/m^2. The PhNR amplitude was measured from the baseline to the negative trough between the cone b-waves and i-waves.

Therefore, we consider that $A\beta_{1-40}$ in wild-type and PS-1 knock-in mouse retinas were detected, and each value in retina includes some extent of endogenous $A\beta_{1-40}$. Although we did not measure $A\beta_{1-42}$ in the retina using ELISA in this study, it is known that $A\beta_{1-40}$ requires aggregated $A\beta_{1-42}$ as a core protein to form insoluble forms, and therefore an accumulation of $A\beta_{1-42}$ in the retina may be predicted (Hasegawa *et al.* 1999). Collectively, these findings suggest that APP/PS-1 mice aged from 11 to 24 months accumulate insoluble forms of Aβ in the retina as well as in the brain.

To investigate the expression and localization of $A\beta_{1-42}$ in the retina, we examined retinas immunohistochemically using an $A\beta_{1-42}$-specific antibody (FCA3542) (Barelli *et al.* 1997). Interestingly, $A\beta_{1-42}$ immunoreactivity was markedly accumulated which the intracellular space, notably of the cell body, in GCL, inner nuclear layer, and outer nuclear layer in both APP Tg and APP/PS-1 Tg mouse retinas at 24-months old, with little immunoreactivity being seen in age-matched wild-type mouse retinas. On the other hand, no amyloid plaques were detected in retinas of APP or APP/PS-1 Tg mice at 24-months old using the $A\beta_{1-42}$-specific antibody (FCA3542) or thioflavin-S staining (Shimazawa M. and Hara H., unpublished data). These results are novel because $A\beta_{1-42}$ was previously known to form amyloid plaques in the brain (Hsiao *et al.* 1996), and indeed, we confirmed that APP/PS-1 double Tg mice exhibit amyloid plaques within the brain at 8-months old and later (Shimazawa M. and Hara H., unpublished data). As one of the reason why, it is considered that insoluble Aβ levels in retina of APP/PS-1 Tg mice are at least 30 times lower than those in brain. Senile plaques are a defining neuropathological hallmark of Alzheimer's disease – with the major constituent of plaques (namely, Aβ) being considered to play an important role in the pathophysiology of Alzheimer's disease – and intraneuronal $A\beta_{1-42}$ accumulation is also associated with neurodegeneration (Chui *et al.* 2001; Billings *et al.* 2005). Actually, Wirths *et al.* (2001) noted that intracellular Aβ staining precedes plaque deposition in a double transgenic mouse model expressing human mutant APP and human mutant PS-1. Taken together, these findings suggest that intraneuronal Aβ accumulation in the retina may affect physiological regulation.

Walsh *et al.* (2002, 2005) have reported that the chronic activation of glial cells induced by a single intravitreal injection of $A\beta_{1-42}$ peptide results in a chronic atrophy of neurons in the rat retina. In the present study, there were no significant differences in GCL cell number or IPL thickness between any of the Tg mice and age-matched wild-type mice at 12-months old. Several lines of evidence suggest that Aβ toxicity may be related to elevated levels of glutamate and/or to overactivity of NMDA receptors (Koh *et al.* 1990; Gray and Patel 1995; Masliah *et al.* 2000; Qiu and Gruol 2003). Indeed, the cellular damage seen in the Alzheimer's brain is especially prominent in areas that display glutamatergic synaptic plasticity (Arendt *et al.* 1998). However, APP Tg and APP/PS-1 double Tg mice, but not PS-1 Tg mice, displayed less retinal damage after NMDA injection than age-matched wild-type mice at 15-months old. Furthermore, the number of TUNEL-positive cells was significantly less in ganglion cell layer of APP/PS-1 Tg mice than PS-1 Tg mice 24 h after NMDA injection. To clarify whether Aβ or APP participates in the reduced retinal damages, we examined the effect of DAPT, a γ-secretase inhibitor, on NMDA-induced retinal damages and compared their effects between PS-1 and APP/PS-1 Tg mice. Ttreatment with DAPT at 100 mg/kg s.c. (3 h before and just after NMDA) significantly diminished the reduced damages in APP/PS-1 Tg mice. In the previous study, DAPT (10, 30 and 100 mg/kg, s.c.) dose-dependently reduced Aβ levels in the cerebrospinal fluid and plasma of Tg2576 mice (Lanz *et al.* 2003). Furthermore, Comery at al. (Comery *et al.* 2005) reported that acute treatment before training (but not after training or before testing) with DAPT, at a dose that reduces brain concentrations of Aβ (100 mg/kg, p.o.), attenuated the memory impairment in 20- to 65-week-old Tg2576 mice. These data strongly indicate that either the NMDA receptor itself or its downstream signals may be attenuated by Aβ.

Retinal ganglion cells are exquisitely sensitive to the effects of both glutamate and its analog NMDA, which produces a dose-dependent cell-loss both *in vivo* and *in vitro*, and glutamate toxicity has been implicated in the pathophysiology of glaucoma (Dreyer 1998). Furthermore, it is well established that neuronal CaMKII is regulated by Ca^{2+} influx via NMDA receptors (Fukunaga *et al.* 1992, 1993). To look for evidence of differences in the NMDA receptor and/or its downstream signaling in APP/PS-1 double Tg mice, we examined the changes in expression and localization of the NMDA-receptor 1 (NR1) subunit and in the phosphorylated form of CaMKIIα (p-CaMKIIα) as a downstream signaling molecule. Although NR1 protein did not show any change in level in the retinas of APP/PS-1 mice (vs. wild-type mice), the condensed localizations seen within GCL cell bodies in PS-1 knock-in mice (used as control mice) were not evident

in APP or APP/PS-1 Tg mice. Furthermore, we measured NMDA-receptor 2A (NR2A) and 2B (NR2B) protein levels in retinal membrane extracts of APP/PS-1 double Tg and compared with age-matched wild-type mice. NR2B protein in retinal membrane fraction, but not total retinal extracts, was significantly decreased in APP/PS-1 double Tg mice as compared with wild-type mice. Although there was no difference in NR2A protein of total retinal extracts between APP/PS-1 double Tg mice and wild-type mice, we could not detect it in retinal membrane fraction of both mice (Shimazawa *et al.*, 2008, unpublished data). These results indicate that NR1/NR2B heterodimers may dominantly exist in retinal membrane and NR2B protein is decreased in APP/PS-1 double Tg mice as compared with wilt-type mice. Furthermore, these data suggest that the localization of NMDA receptors on the retinal cell surface may be reduced in APP/PS-1 double Tg mice. A large number of studies have reported that Aβ reduces normal neurotransmission in brain neuron (Nakagami and Oda 2002; Wang *et al.* 2004; Snyder *et al.* 2005; Goto *et al.* 2006; Chin *et al.* 2007; Venkitaramani *et al.* 2007). In line with these findings: (a) Snyder *et al.* (2005) found that $A\beta_{1-42}$ promoted endocytosis of NMDA receptors in cortical neurons, and that it produced a rapid and persistent depression of NMDA-evoked currents, while (b) Goto *et al.* (2006) reported that pre-treatment with $A\beta_{1-42}$ significantly reduced the cell-surface expression of NR1, but not the total NR1 level, and that it protects against glutamate-induced extracellular calcium influx and cell death in rat cultured hippocampal neurons. Furthermore, we found that both p-CaMKIIα in the retinal extracts and total CaMKIIα in retinal membrane fraction were reduced in APP/PS-1 double Tg mice as compared with age-matched wild-type mice, and our immunohistochemistry revealed that the p-CaMKIIα level within GCL cells was markedly reduced in APP and APP/PS-1 double Tg mice. CaMKIIα is translocated from the cytosolic fraction to the membrane fraction following binding to NMDA-receptor subunits (NR1 and NR2B) and its phosphorylation (Colbran 2004). These findings support the idea that the reduced CaMKIIα level in the membrane fraction reflects a decrease in p-CaMKIIα level in the retina. Further, we found that injection of NMDA at 5 nmol/eye increased p-CaMKIIα in retinas obtained from wild-type mice, with it is a smaller increase being seen in retinas obtained from APP/PS-1 double Tg mice. Collectively, these results indicate that NMDA signals are attenuated in the retina of the APP/PS-1 double Tg mouse.

Patients with Alzheimer's disease have been reported to exhibit a longer latency to the P2 component of flash VEPs (Jackson and Owsley 2003), and thus visual dysfunction in Alzheimer's patients is believed to be more reflective of cortical disturbances than of Alzheimer's disease-associated optic neuropathy. In the present study, the latencies, but not the amplitudes, of the P1 and N1 components of the flash VEP were greater in APP/PS-1 mice than in age-matched wild-type mice. In addition, ERG recordings to assess retinal function revealed longer latencies of both a-wave reflecting activity of the photoreceptors in the outer retina and oscillation potentials reflecting activity in amacrine cells in scotopic condition, and decrease in amplitude of photopic negative response (PhNR) reflecting inner retinal function such as RGC and amacrine cells in APP/PS-1 mice than in age-matched wild-type mice. These findings suggest that retinal dysfunctions may occur in APP/PS-1 mice, and also that the reduction in NMDA-receptor signaling induced by Aβ accumulation may form part of the underlying mechanisms. On the other hand, the delayed latency in a-wave reflecting photoreceptor function could not be explained by the reduction in NMDA-receptor signaling. Therefore, further studies are needed to clarify the mechanisms for visual dysfunction in APP/PS-1 double Tg mice. This is the first report that visual dysfunctions were demonstrated in Alzheimer's model mice such as APP/PS-1 double Tg mice. Since some behavioral responses in these mice are evaluated as an index of memory deficits, the visual dysfunction may affect the memory deficits obtained from the behavioral outcome.

In conclusion, we are reporting evidence suggesting that exposure to Aβ may reduce activation of NMDA-receptor signaling pathways and lead to retinal dysfunction. Our findings may indicate a potential new target for therapeutic interventions against retinal diseases.

Acknowledgments

This study was supported by a research grant from the Ministry of Education, Culture, Sports Science and Technology of the Japanese Government (No. 18659515). The authors wish to express their gratitude to Mr. Atsushi Oyagi for skillful technical assistance.

Supporting information

Additional supporting information may be found in the online version of this article.

Appendix S1 Experimental procedures – ELISA (enzyme-linked immunosorbent assay) in fore brain.

Fig. S1 Concentrations of amyloid-β (Aβ)1–40 and Aβ1–42 in soluble and insoluble fractions of forebrain extracts in human mutant amyloid precursor protein transgenic (Tg) mice (Tg 2576), mutant presenilin-1 (PS-1) knock-in mice, APP/PS-1 double Tg mice, and wild-type mice.

Fig. S2 Histological comparisons of non-treated retinas from human mutant amyloid precursor protein (APP) transgenic (Tg) mice (Tg 2576), mutant presenilin-1 (PS-1) knock-in mice, APP/PS-1 double Tg mice, and wild-type mice.

Fig. S3 Phosphorylated form of calcium/calmodulin-dependent protein kinase IIα (p-CaMKIIα) and total CaMKIIα in retinas of mutant presenilin-1 (PS-1) knock-in mice and human mutant amyloid precursor protein (APP) and PS-1 (APP/PS-1) double transgenic (Tg) mice after NMDA injection.

Fig. S4 Retinal function in human mutant amyloid precursor protein (APP) and mutant presenilin-1 (PS-1) double transgenic

(APP/PS-1 double Tg) mice and wild-type mice as revealed using electroretinogram (ERG) recordings.

Fig. S5 Visual function in human mutant amyloid precursor protein (APP) and mutant presenilin-1 (PS-1) double transgenic (APP/PS-1 Tg) mice and wild-type mice as revealed using visual-evoked potential (VEP) recordings.

Please note: Blackwell Publishing is not responsible for the content or functionality of any supporting materials supplied by the authors. Any queries (other than missing material) should be directed to the corresponding author for the article.

References

Arendt T., Bruckner M. K., Gertz H. J. and Marcova L. (1998) Cortical distribution of neurofibrillary tangles in Alzheimer's disease matches the pattern of neurons that retain their capacity of plastic remodelling in the adult brain. *Neuroscience* **83**, 991–1002.

Barelli H., Lebeau A., Vizzavona J. *et al.* (1997) Characterization of new polyclonal antibodies specific for 40 and 42 amino acid-long amyloid beta peptides: their use to examine the cell biology of presenilins and the immunohistochemistry of sporadic Alzheimer's disease and cerebral amyloid angiopathy cases. *Mol. Med.* **3**, 695–707.

Bayer A. U., Ferrari F. and Erb C. (2002) High occurrence rate of glaucoma among patients with Alzheimer's disease. *Eur. Neurol.* **47**, 165–168.

Billings L. M., Oddo S., Green K. N., McGaugh J. L. and LaFerla F. M. (2005) Intraneuronal Aβ causes the onset of early Alzheimer's disease-related cognitive deficits in transgenic mice. *Neuron* **45**, 675–688.

Bonne C., Muller A. and Villain M. (1998) Free radicals in retinal ischemia. *Gen. Pharmacol.* **30**, 275–280.

Chin J. H., Ma L., MacTavish D. and Jhamandas J. H. (2007) Amyloid β protein modulates glutamate-mediated neurotransmission in the rat basal forebrain: involvement of presynaptic neuronal nicotinic acetylcholine and metabotropic glutamate receptors. *J. Neurosci.* **27**, 9262–9269.

Chui D. H., Dobo E., Makifuchi T. *et al.* (2001) Apoptotic neurons in Alzheimer's disease frequently show intracellular Aβ42 labeling. *J. Alzheimers. Dis.* **3**, 231–239.

Colbran R. J. (2004) Targeting of calcium/calmodulin-dependent protein kinase II. *Biochem. J.* **378**, 1–16.

Comery T. A., Martone R. L., Aschmies S. *et al.* (2005) Acute γ-secretase inhibition improves contextual fear conditioning in the Tg2576 mouse model of Alzheimer's disease. *J. Neurosci.* **25**, 8898–8902.

Dentchev T., Milam A. H., Lee V. M., Trojanowski J. Q. and Dunaief J. L. (2003) Amyloid-β is found in drusen from some age-related macular degeneration retinas, but not in drusen from normal retinas. *Mol. Vision* **9**, 184–190.

Dreyer E. B. (1998) A proposed role for excitotoxicity in glaucoma. *J. Glaucoma* **7**, 62–67.

Dreyer E. B., Zurakowski D., Schumer R. A., Podos S. M. and Lipton S. A. (1996) Elevated glutamate levels in the vitreous body of humans and monkeys with glaucoma. *Arch. Ophthalmol.* **114**, 299–305.

Fukunaga K., Soderling T. R. and Miyamoto E. (1992) Activation of Ca^{2+}/calmodulin-dependent protein kinase II and protein kinase C by glutamate in cultured rat hippocampal neurons. *J. Biol. Chem.* **267**, 22527–22533.

Fukunaga K., Stoppini L., Miyamoto E. and Muller D. (1993) Long-term potentiation is associated with an increased activity of Ca^{2+}/calmodulin-dependent protein kinase II. *J. Biol. Chem.* **268**, 7863–7867.

Goto Y., Niidome T., Akaike A., Kihara T. and Sugimoto H. (2006) Amyloid β-peptide preconditioning reduces glutamate-induced neurotoxicity by promoting endocytosis of NMDA receptor. *Biochem. Biophys. Res. Commun.* **351**, 259–265.

Gray C. W. and Patel A. J. (1995) Neurodegeneration mediated by glutamate and β-amyloid peptide: a comparison and possible interaction. *Brain Res.* **691**, 169–179.

Guo L., Salt T. E., Luong V. *et al.* (2007) Targeting amyloid-β in glaucoma treatment. *Proc. Natl Acad. Sci. USA* **104**, 13444–13449.

Hara H., Oh-hashi K., Yoneda S., Shimazawa M., Inatani M., Tanihara H. and Kiuchi K. (2006) Elevated neprilysin activity in vitreous of patients with proliferative diabetic retinopathy. *Mol. Vision* **12**, 977–982.

Harkany T., Abraham I., Timmerman W. *et al.* (2000) β-amyloid neurotoxicity is mediated by a glutamate-triggered excitotoxic cascade in rat nucleus basalis. *Eur. J. Neurosci.* **12**, 2735–2745.

Hasegawa K., Yamaguchi I., Omata S., Gejyo F. and Naiki H. (1999) Interaction between Aβ (1–42) and Aβ (1–40) in Alzheimer's β-amyloid fibril formation in vitro. *Biochemistry* **38**, 15514–15521.

Hsiao K., Chapman P., Nilsen S., Eckman C., Harigaya Y., Younkin S., Yang F. and Cole G. (1996) Correlative memory deficits, Aβ elevation, and amyloid plaques in transgenic mice. *Science* **274**, 99–102.

Jackson G. R. and Owsley C. (2003) Visual dysfunction, neurodegenerative diseases, and aging. *Neurol. Clin.* **21**, 709–728.

Johnson L. V., Leitner W. P., Rivest A. J., Staples M. K., Radeke M. J. and Anderson D. H. (2002) The Alzheimer's Aβ-peptide is deposited at sites of complement activation in pathologic deposits associated with aging and age-related macular degeneration. *Proc. Natl Acad. Sci. USA* **99**, 11830–11835.

Koh J. Y., Yang L. L. and Cotman C. W. (1990) β-amyloid protein increases the vulnerability of cultured cortical neurons to excitotoxic damage. *Brain Res.* **533**, 315–320.

Lanz T. A., Himes C. S., Pallante G., Adams L., Yamazaki S., Amore B. and Merchant K. M. (2003) The γ-secretase inhibitor *N*-[*N*-(3,5-difluorophenacetyl)-L-alanyl]-*S*-phenylglycine *t*-butyl ester reduces Aβ levels in vivo in plasma and cerebrospinal fluid in young (plaque-free) and aged (plaque-bearing) Tg2576 mice. *J. Pharmacol. Exp. Ther.* **305**, 864–871.

Masliah E., Alford M., Mallory M., Rockenstein E., Moechars D. and Van Leuven F. (2000) Abnormal glutamate transport function in mutant amyloid precursor protein transgenic mice. *Exp. Neurol.* **163**, 381–387.

McKinnon S. J., Lehman D. M., Kerrigan-Baumrind L. A. *et al.* (2002) Caspase activation and amyloid precursor protein cleavage in rat ocular hypertension. *Invest. Ophthalmol. Vis. Sci.* **43**, 1077–1087.

Merrill M. A., Chen Y., Strack S. and Hell J. W. (2005) Activity-driven postsynaptic translocation of CaMKII. *Trends Pharmacol. Sci.* **26**, 645–653.

Nakagami Y. and Oda T. (2002) Glutamate exacerbates amyloid β1–42-induced impairment of long-term potentiation in rat hippocampal slices. *Jpn. J. Pharmacol.* **88**, 223–226.

Nakano Y., Kondoh G., Kudo T., Imaizumi K., Kato M., Miyazaki J. I., Tohyama M., Takeda J. and Takeda M. (1999) Accumulation of murine amyloidβ42 in a gene-dosage-dependent manner in PS1 'knock-in' mice. *Eur. J. Neurosci.* **11**, 2577–2581.

Neufeld A. H. (1999) Nitric oxide: a potential mediator of retinal ganglion cell damage in glaucoma. *Surv. Ophthalmol.* **43**(Suppl. 1), S129–S135.

Qiu Z. and Gruol D. L. (2003) Interleukin-6, β-amyloid peptide and NMDA interactions in rat cortical neurons. *J. Neuroimmunol.* 139, 51–57.

Shimazawa M., Inokuchi Y., Ito Y., Murata H., Aihara M., Miura M., Araie M. and Hara H. (2007a) Involvement of ER stress in retinal cell death. *Mol. Vision* **13**, 578–587.

Shimazawa M., Ito Y., Inokuchi Y. and Hara H. (2007b) Involvement of double-stranded RNA-dependent protein kinase in ER stress-induced retinal neuron damage. *Invest. Ophthalmol. Vis. Sci.* **48**, 3729–3736.

Snyder E. M., Nong Y., Almeida C. G. *et al.* (2005) Regulation of NMDA receptor trafficking by amyloid-β. *Nat. Neurosci.* **8**, 1051–1058.

Suemori S., Shimazawa M., Kawase K., Satoh M., Nagase H., Yamamoto T. and Hara H. (2006) Metallothionein, an endogenous antioxidant, protects against retinal neuron damage in mice. *Invest. Ophthalmol. Vis. Sci.* **47**, 3975–3982.

Venkitaramani D. V., Chin J., Netzer W. J., Gouras G. K., Lesne S., Malinow R., Lombroso P. J. (2007) β-amyloid modulation of synaptic transmission and plasticity. *J. Neurosci.* **27**, 11832–11837.

Viswanathan S., Frishman L. J. and Robson J. G. (2000) The uniform field and pattern ERG in macaques with experimental glaucoma: removal of spiking activity. *Invest. Ophthalmol. Vis. Sci.* **41**, 2797–2810.

Viswanathan S., Frishman L. J., Robson J. G. and Walters J. W. (2001) The photopic negative response of the flash electroretinogram in primary open angle glaucoma. *Invest. Ophthalmol. Vis. Sci.* **42**, 514–522.

Walsh D. T., Montero R. M., Bresciani L. G. *et al.* (2002) Amyloid-β peptide is toxic to neurons in vivo via indirect mechanisms. *Neurobiol. Dis.* **10**, 20–27.

Walsh D. T., Bresciani L., Saunders D., Manca M. F., Jen A., Gentleman S. M. and Jen L. S. (2005) Amyloid β peptide causes chronic glial cell activation and neuro-degeneration after intravitreal injection. *Neuropathol. Appl. Neurobiol.* **31**, 491–502.

Wang Q., Rowan M. J. and Anwyl R. (2004) β-amyloid-mediated inhibition of NMDA receptor-dependent long-term potentiation induction involves activation of microglia and stimulation of inducible nitric oxide synthase and superoxide. *J. Neurosci.* **24**, 6049–6056.

Wirths O., Multhaup G., Czech C., Blanchard V., Moussaoui S., Tremp G., Pradier L., Beyreuther K. and Bayer T. A. (2001) Intraneuronal Aβ accumulation precedes plaque formation in beta-amyloid precursor protein and presenilin-1 double-transgenic mice. *Neurosci. Lett.* **306**, 116–120.

Yamamoto R., Yoneda S. and Hara H. (2004) Neuroprotective effects of β-secretase inhibitors against rat retinal ganglion cell death. *Neurosci. Lett.* **370**, 61–64.

Yoneda S., Hara H., Hirata A., Fukushima M., Inomata Y. and Tanihara H. (2005) Vitreous fluid levels of beta-amyloid$_{(1-42)}$ and tau in patients with retinal diseases. *Jpn. J. Ophthalmol.* **49**, 106–108.

Journal of Cerebral Blood Flow & Metabolism (2008) 28, 354–366

www.jcbfm.com

Propofol exerts greater neuroprotection with disodium edetate than without it

Yoshinori Kotani[1,2], Yoshimi Nakajima[1], Tatsuya Hasegawa[3], Masahiko Satoh[4], Hisamitsu Nagase[4], Masamitsu Shimazawa[1], Shinichi Yoshimura[2], Toru Iwama[2] and Hideaki Hara[1]

[1]*Department of Biofunctional Molecules, Gifu Pharmaceutical University, Gifu, Japan;* [2]*Department of Neurosurgery, Gifu University Graduate School of Medicine, Gifu, Japan;* [3]*The Yamanashi Institute of Environmental Sciences, Yamanashi, Japan;* [4]*Department of Hygiene, Gifu Pharmaceutical University, Gifu, Japan*

The main objective of this study, on mice, was to compare the neuroprotective effects of propofol with those of propofol plus disodium edetate (propofol EDTA). We also administered propofol EDTA (0.005% (w/v) EDTA) to mice intravenously, and measured the changes in zinc concentrations occurring after permanent middle cerebral artery occlusion. In the *in vivo* study, propofol EDTA displayed stronger neuroprotective effects than propofol alone. Furthermore, we examined the neuroprotective effects of EDTA administered alone, and found that EDTA Na significantly reduced the infarct volume. The number of terminal deoxynucleotidyl transferase-mediated dUTP nick end-labeling-positive cells in the ischemic penumbra was reduced more by propofol EDTA than by propofol alone. We performed in the *in vitro* study in five groups (aerobic, vehicle (control), propofol, EDTA, and propofol plus EDTA). Propofol and EDTA each protected PC12 cells against oxygen–glucose deprivation-induced cell damage, and the effect of propofol was increased by adding EDTA. Because the chelating action of EDTA was a potential causal mechanism, we examined the effect of propofol EDTA on intracerebral zinc homeostasis. When propofol EDTA was given intravenously 10 mins before cerebral ischemia, the zinc concentration decreased significantly in the cortical area, but not in the subcortex. In conclusion, (a) propofol provides neuroprotection against both *in vivo* and *in vitro* ischemic damage, and its effects are enhanced when EDTA is added; and (b) EDTA itself protects against ischemic neuronal damage, possibly, owing to its zinc-chelating action.
Journal of Cerebral Blood Flow & Metabolism (2008) **28,** 354–366; doi:10.1038/sj.jcbfm.9600532; published online 25 July 2007

Keywords: chelation; disodium edetate (EDTA); middle cerebral artery occlusion; propofol; zinc

Introduction

Propofol (2,6-diisopropylphenol) is a potent intravenous hypnotic agent, and is widely used both for the induction and maintenance of anesthesia as well as for sedation in the intensive care unit (Marik, 2004). Laboratory investigations have revealed that propofol might also protect the brain against ischemic injury. Numerous characteristics of propofol have been reported: (a) it reduces cerebral blood flow, the cerebral metabolic rate for oxygen, and intracranial pressure (Pittman *et al*, 1997); (b) it acts as an antioxidant, directly scavenges free radicals, and decreases lipid peroxidation (Sagara *et al*, 1999; Wilson and Gelb, 2002); (c) it activates γ-aminobutyric acid type A receptors (Ito *et al*, 1999), inhibits glutamate receptors (Zhan *et al*, 2001), and reduces the extracellular glutamate concentration via an inhibition of Na^+ channel-dependent glutamate release or an enhancement of glutamate uptake (Sitar *et al*, 1999); and (d) it reportedly reduces ischemic neuronal injury in animal models of transient global and focal cerebral ischemia (Young *et al*, 1997), although conflicting results have been obtained in studies carried out using models of permanent middle cerebral artery occlusion (MCAO). Indeed, although Tsai *et al* (1994) failed to show a protective action of propofol after permanent MCAO in the same model, Adembri *et al* (2006) reported that it reduced infarct size.

This study was therefore designed to evaluate the neuroprotective properties of propofol, primarily by determining whether it alters the volume of the

Correspondence: Professor Dr H Hara, Department of Biofunctional Molecules, Gifu Pharmaceutical University, 5-6-1 Mitahora-higashi, Gifu 502-8585, Japan.
E-mail: hidehara@gifu-pu.ac.jp
Received 16 January 2007; revised 11 May 2007; accepted 19 June 2007; published online 25 July 2007

infarct resulting from permanent focal cerebral ischemia in mice. For the following reasons, we also (a) asked whether a modulating influence over the neuroprotective effects of propofol might be exerted by disodium edetate (EDTA) and (b) tested the effects of EDTA on intracerebral zinc concentrations during the cerebral ischemia. The physiologic significance of neuronal zinc release within the central nervous system is not clear, moreover, its role in ischemic brain injury is controversial (Shabanzadeh *et al*, 2004). Indeed, although Miyawaki *et al* (2004) concluded that the synaptic release of Zn^{2+}, which is potently neurotoxic and its translocation into postsynaptic neurons might be implicated in ischemic cell death, other authors (Matsushita *et al*, 1996) stress that zinc may have a protective function. EDTA, which is usually included in pharmaceutical preparation of propofol to retard bacterial and fungal growth, has the ability to chelate almost every positive ion in the periodic table. We hypothesized that chelation of excessive neuronal zinc might ameliorate zinc-induced neurotoxicity and reduce subsequent neuronal injury. We therefore compared the neuroprotective effects of propofol EDTA and propofol alone. Because the presence of EDTA enhanced the neuroprotective effects of propofol, determined of the intracerebral zinc concentrations to know whether EDTA exerted this modulating effect by chelating surplus intracerebral zinc.

Materials and methods

Animals

The experiments were conducted in accordance with the Animal Care Guidelines issued by the Animal Experiments Committee of Gifu Pharmaceutical University. All efforts were made to minimize both suffering and the number of animals used. All *in vivo* experiments were performed using male ddY mice (5-week old; body weight 26 to 32 g; Japan SLC Ltd., Shizuoka, Japan). The animals were housed at 24±2°C under a 12 h light–dark cycle (lights on from 0700 to 1900). Each animal was used for one experiment only.

Drugs

For this study, 1% Diprivan® injection and 1% Propofol injection 'Maruishi' were purchased from AstraZeneca Co. Ltd. (Osaka, Japan) and Maruishi Co. Ltd. (Osaka, Japan), respectively. Intralipid and EDTA Na were from Terumo Co. Ltd. (Tokyo, Japan) and Sigma (Deisenhofen, Germany), respectively. Pentobarbital and isoflurane were from Nissan Kagaku (Tokyo, Japan) and Merck Hoei Ltd. (Osaka, Japan), respectively. 2,3,5-Triphenyltetrazolium chloride (TTC), ethylenediaminetetraacetic acid (EDTA) disodium salt dihydrate, Dulbecco's modified Eagle's medium, and resazurin were all from Sigma-Aldrich Co. (St Louis, MO, USA). Nitric acid for atomic absorption spectrometry and hydrogen peroxide for atomic absorption spectrochemical analysis were purchased from Kanto Chemical Co. Inc. (Tokyo, Japan) and Wako Pure Chemical Industries (Osaka, Japan), respectively. Hoechst 33342 and YO-PRO-1 were from Molecular Probes (Eugene, OR, USA).

Focal Cerebral Ischemia Model in Mice

Anesthesia was induced using 2.0 to 3.0% isoflurane and maintained using 1.0 to 1.5% isoflurane in 70% N_2O/30% O_2 by means of an animal general anesthesia machine (Soft Lander, Sin-ei Industry Co. Ltd., Saitama, Japan). Body temperature was maintained at 37.0 to 37.5°C with the aid of a heating pad and heating lamp. In each mouse, regional cerebral blood flow was monitored by laser-Doppler flowmetry (Omegaflow flo-N1; Omegawave Inc., Tokyo, Japan). A flexible probe was fixed to the skull (2 mm posterior and 6 mm lateral to bregma). After a midline skin incision, the left external carotid artery was exposed, and its branches were occluded (Hara *et al*, 1996, 1997). An 8-0 nylon monofilament (Ethicon, Somerville, NJ, USA) coated with a mixture of silicone resin (Xantopren; Bayer Dental, Osaka, Japan) was introduced into the left internal carotid artery through the external carotid artery stump so as to occlude the origin of the middle cerebral artery (MCA). Afterwards, the left common carotid artery was occluded. After the surgery, the mice were kept in a cage with a heating lamp, which maintained the cage temperature between 29 and 30°C for another 3 h. Then, the mice were bred in a preoperative condition (24±2°C) until sampling.

Propofol Treatment

Control (vehicle), propofol EDTA, and propofol groups received 10% intralipid, 1% Diprivan® injection (which includes 0.005% (w/v) disodium edetate (EDTA)), and 1% Propofol injection 'Maruishi', respectively. Mice were randomly assigned to one of the three groups to receive propofol with EDTA, propofol alone, or vehicle intravenously (0.1 ml/10 g, over 90 secs) 10 mins before MCAO. Propofol (with or without EDTA) was administered at 1, 5, or 10 mg/kg (total seven groups). In an experiment to examine time dependency, propofol (10 mg/kg, with or without EDTA) or intralipid were administered 10 mins before, after, or 1 h after MCAO (total nine groups). In addition, we prepared another three were groups (intralipid (vehicle), propofol EDTA, and propofol) to evaluate the survival rate, infarct volume, and neurologic deficits at 7 days after MCAO. Mice received propofol (with or without EDTA, 10 mg/kg, intravenously) or intralipid intravenously 10 mins before MCAO.

EDTA Na Treatment

Mice were randomly assigned to receive EDTA Na (0.05 or 0.5 mg/kg) or vehicle intravenously (0.1 ml/10 g, over 90 secs) 10 mins before MCAO.

Physiologic Monitoring

A polyethylene catheter inserted into the left femoral artery was used to measure arterial blood pressure and heart rate (Power Lab/8SP; AD Instrument, Osaka, Japan) 20 mins before and 30 mins after MCAO. Propofol (with or without EDTA) was administered intravenously (10 mg/kg, over 90 secs, 0.1 ml/10 g) at 10 mins before MCAO. Blood samples (50 μL) were taken before and at 30 mins after the onset of ischemia for pharmacokinetic analysis. pH, pCO_2, pO_2, and glucose were measured (i-STAT 300F, Abbot Co., Abbot Park, IL, USA). Regional cerebral blood flow was measured during this period by the method described in the section Focal cerebral ischemia model in mice. Physiologic monitoring was carried out a separate study.

Assessment of Cerebral Infarct and Cerebral Edema Volumes

To analyze infarct volume, mice were euthanized using sodium pentobarbital at 24 h or 7 day after MCAO, and forebrains were sectioned coronally into five slices (2 mm thick) and placed in 2% TTC at 37°C for 30 mins. The infarcted areas were recorded as images using a digital camera (Coolpix 4500, Nikon, Tokyo, Japan), then quantitated (using an Image J), and calculated as in a previous report (Hara *et al*, 1997). Brain swelling was calculated according to the following formula: (infarct volume + ipsilateral undamaged volume–contralateral volume) × 100/contralateral volume (%) (Hara *et al*, 1996).

Neurologic Deficits

Mice were tested for neurologic deficits at 24 h or 7 day after MCAO and scored as described in our previous study (Hara *et al*, 1996) using the following scale: 0, no observable neurologic deficits (normal); 1, failure to extend the right forepaw (mild); 2, circling to the contralateral side (moderate); 3, loss of walking or righting reflex (severe). The investigator who rated the mice was masked as to the group to which each mouse belonged.

Terminal Deoxynucleotidyl Transferase-Mediated dUTP Nick End-Labeling Staining

The terminal deoxynucleotidyl transferase-mediated dUTP nick end-labeling staining (TUNEL) assay was performed according to the manufacturer's instructions (Roche Molecular Biochemicals Inc., Mannheim, Germany). Ischemic areas of cortical brain sections of 0.4 to 1.0 mm anterior to bregma (through the anterior commissure) were excised and used. For this part of the study, we referred to a mouse brain atlas (George Paxinos and Keith BJ Franklin, *The Mouse Brain in Stereotaxic Coordinates*, 2nd edition, 2001). Paraffin-embedded sections were dewaxed and rehydrated, and then incubated in 20 mg/ml of proteinase K for 30 mins. After immersion in 100 μml of 3% H_2O_2 for 30 mins, sections were incubated in a terminal deoxynucleotidyl transferase (TdT) labeling reaction mixture (supplied with the kit) in a humidified chamber for 90 mins at 37°C, then incubated in the stop buffer at 37°C for 4 mins.

Cell Counting

To quantify the number of DNA-fragmented cells present after MCAO, the numbers of TUNEL-positive cells in the caudate-putamen (as the ischemic core) and cortex (as the ischemic penumbra; two areas, the superior and inferior cortical areas) were counted in a high-powered field (× 200) on a section through the anterior commissure by a masked investigator. Each count was expressed as number/mm^2 ($n = 6$ or 7).

Measurement of Intracerebral Zinc Concentrations

Forty mice were assigned to the following experimental groups (10 mice per group): (1) vehicle (no ischemia) group; (2) propofol EDTA (no ischemia) group; (3) vehicle (ischemia) group; and (4) propofol EDTA (ischemia) group. Propofol EDTA (10 mg/kg) or vehicle was administered intravenously (0.1 ml/10 g, over 90 secs) 10 mins before MCAO, and mice were euthanized using sodium pentobarbital at 1 h after MCAO. Non-ischemic groups were killed 1 h after administration of drug or vehicle. The resected brain was promptly divided into cortex and subcortex under a microscope. The areas perfused by the anterior cerebral artery and posterior cerebral artery were then removed from the cortexes. The resected samples were incubated at 100°C for 24 h to remove edema, and dry samples were weighed. The concentration of zinc present in each tissue was determined using the following method. Two milliliters of nitric acid was added to each dried sample followed by gradual heating from 70 to 140°C. The following day, 0.5 ml of nitric acid and 2 ml of H_2O_2 were added to each sample, followed (as before) by gradual heating from 70 to 140°C. The dry samples were brought to 4.0 ml with deionized water, and the zinc concentration in the samples was determined using ICP-MS (HP 4500; Yokokawa Analytical Systems, Tokyo, Japan). Mass numbers of *m*/z 64 and 66 m/z were used for these determinations.

Cell Culture

PC12 cells were maintained in Dulbecco's modified Eagle's medium supplemented with 10% heat-inactivated horse serum and 5% heat-inactivated fetal bovine serum at 37°C under a humidified 5% CO_2 atmosphere. To examine the effect of propofol on oxygen–glucose deprivation (OGD)-induced cell death, cells were seeded into collagen-coated 24-well plates at a density of 1×10^4 cells/well. After incubating for 7 days, the culture medium was removed and the cells, after being washed twice with glucose-free Dulbecco's modified Eagle's medium, were incubated in the same glucose-free medium for 4 h in an oxygen-free incubator (94% N_2, 5% CO_2, and 1% O_2). After OGD, sufficient glucose was added to bring it to the normal level (final concentration, 4.5 mg/ml) and cells

were incubated under normal growth conditions for an additional 18 h (reoxygenation). Propofol (10 or 20 μmol/L) or EDTA (0.05 μmol/L) was added to the glucose-free medium before OGD treatment.

Cell Viability

The first method used here for assessing cell viability was a single-cell digital imaging-based method employing fluorescent staining of nuclei. Cell death was assessed on the basis of combination staining with fluorescent dyes (namely, Hoechst 33342 and YO-PRO-1 (Molecular Probes)), observations being made using an inverted epifluorescence microscope (Olympus, Tokyo, Japan). YO-PRO-1 (λ_{ex} 491 nm and λ_{em} >509 nm), a membrane-impermeant dye, is generally excluded from viable cells, whereas early-stage apoptotic and necrotic cells are YO-PRO-1-positive. At the end of the culture period, Hoechst 33342 and YO-PRO-1 dyes were added to the culture medium (at 8 and 0.1 μmol/L, respectively) for 30 mins. Images were collected using a digital camera (Coolpix 4500). In a blind manner, a total of at least 400 cells per condition were counted using image-processing software (Image-J ver. 1.33f; National Institutes of Health, Bethesda, MD, USA). Cell mortality was quantified by determining the percentage of cells that were YO-PRO-1-positive (Hoechst 33342-positive cells being taken as the total number of cells present, as Hoechst 33342 stains are both live and dead cells).

Second, we examined the change in fluorescence intensity after cellular reduction of resazurin to resorufin. All experiments were performed in Dulbecco's modified Eagle's medium at 37°C. Cell viability was assessed after immersion in 10% resazurin solution for 3 h at 37°C, and fluorescence was recorded at 560/590 nm.

Statistical Analysis

All data are presented as mean±s.d. Statistical comparisons were made using a one- or two-way analysis of variance followed by Student's *t*-test, Dunnett's test, Bonferroni correction, or the Mann–Whitney *U*-test. A χ^2 test was used to identify differences in the survival rates. StatView software version 5.0 (SAS Institute Inc., Cary, NC, USA) was used. $^*P<0.05$ was considered statistically significant.

Results

Physiologic Parameters

Physiologic parameters are shown for all groups in Table 1. There were no significant differences in regional cerebral blood flow, mean arterial blood pressure, or heart rate, or in arterial pH, pCO_2, pO_2, or glucose among the vehicle, propofol, and propofol with EDTA groups. Surface regional cerebral blood flow was reduced to 19 to 22% of baseline regional cerebral blood flow immediately after MCAO in all mice. Glucose was increased to 142 to 143% of preischemic value after MCAO in all mice.

Infarction, Edema, and Neurologic Deficits

Using TTC staining, we examined whether propofol EDTA and propofol would reduce infarct volume. Twenty-four hours after MCAO, the mice had developed infarcts affecting the cortex and striatum. Mice that died within 24 h after the operation were excluded from the present experiment. Five of 42 (11.9% mortality), five of 64 (7.8%), and seven of 63 (11.1%) mice died in the intralipid, propofol EDTA, and propofol treatment groups, respectively. No significant differences in mortality rate were observed among the treatment groups. First, each drug preparation was administered intravenously 10 mins before MCAO. Administration of 5 or 10 mg/kg propofol EDTA or propofol (but not 1 mg/kg)

Table 1 Physical parameters before and after drug administration

Parameters	*Vehicle*		*Propofol EDTA*		*Propofol*	
	Before ischemia	*After ischemia*	*Before ischemia*	*After ischemia*	*Before ischemia*	*After ischemia*
rCBF (ml/min per 100 g)	72.9±8.4	15.6±7.8	74.4±9.7	14.3±3.4	64.7±6.9	12.5±2.3
(%)	100	21.3±10.1	100	19.4±2.3	100	19.1±4.2
MABP (mm Hg)	65.2±11.2	69.8±13.0	69.7±12.5	68.3±11.4	68.4±11.4	69.1±12.6
HR (beats/min)	468.3±57.2	449.8±72.2	502.0±92.2	484.4±72.3	517.2±66.0	487.7±38.3
pH	7.34±0.09	7.29±0.06	7.41±0.04	7.34±0.07	7.37±0.02	7.32±0.07
pCO_2 (mm Hg)	34.6±11.6	36.7±11.4	34.5±7.8	33.3±11.1	36.9±2.5	36.5±9.1
pO_2 (mm Hg)	132.6±34.2	114.0±29.1	139.8±11.0	142.0±29.2	123.4±20.9	127.4±27.3
Glucose (mg/dL)	216.6±52.1	307.4±67.5	211.0±37.0	302.2±56.6	221.2±35.0	314.2±54.0
(%)	100	142.5±8.6	100	143.0±3.2	100	142.3±15.1

ANOVA, analysis of variance; MCA, middle cerebral artery.
Values are mean±s.d. ($n = 5$). Regional cerebral blood pressure (rCBF) was monitored by laser-Doppler flowmetry using a flexible probe fixed to the skull (2 mm posterior and 6 mm lateral to bregma). Mean arterial blood pressure (MABP) and heart rate (HR) were measured at 20 mins before and 30 mins after MCA occlusion. Propofol (with or without EDTA) was administered intravenously (10 mg/kg, over 90 secs, 0.1 ml/10 g) at 10 mins before MCA occlusion. Blood samples were taken before and at 30 mins after the onset of ischemia for pharmacokinetic analysis (pH, pCO_2, pO_2, and glucose being measured). There were no significant differences among the vehicle, propofol EDTA, and propofol groups (two-way ANOVA).

significantly reduced infarct area, infarct volume, and brain swelling (Figures 1A to 1C), with propofol EDTA reducing infarct area and brain swelling significantly more than propofol. Similarly, propofol EDTA or propofol administered at 5 or 10 mg/kg (intravenously at 10 mins before ischemia), but not at 1 mg/kg, apparently reduced the neurologic deficits, although only propofol EDTA reduced them significantly (Figure 1D).

Next, we reviewed the time dependency of the drug efficacy of propofol EDTA and propofol. Propofol EDTA and propofol (10 mg/kg intravenously at 10 mins before or after MCAO) apparently decreased the cerebral infarction, whereas no clear effects were observed in the groups treated at 1 h after MCAO. Indeed, propofol EDTA and propofol, when administered 10 mins before MCAO, each significantly reduced infarct volume and brain swelling (Figures 2A and 2B). When propofol EDTA was administered after MCAO, infarct area and infarct volume were significantly reduced, but brain swelling was not (versus vehicle-treated mice). When administered after MCAO, propofol alone also displayed a neuroprotective effect, but the effect, was if any, weaker than that of propofol EDTA. When propofol EDTA or propofol was administered 1 h after MCAO, there was no reduction in infarct area, infarct volume, and brain swelling (edema) (versus vehicle-treated mice). The mortality rate, infarct volume, and neurologic deficit scores after MCAO were compared among the treatment groups when examined over a 7-day period. Seven of 15 (46.7% mortality), 6 of 13 (46.2%), and 7 of 14 (50.0%) mice died in the intralipid, 10 mg/kg propofol EDTA, and 10 mg/kg propofol treatment groups, respectively. No significant differences in mortality rate were observed among the treatment groups. Moreover, propofol EDTA decreased infarct volume significantly at 7 days after MCAO (versus vehicle) (Figure 3A). Thus, overall propofol EDTA displayed greater neuroprotection than propofol.

Similarly, administration of propofol EDTA at 10 mins before (but not at, after, or 1 h after) MCAO led to a significant reduction in the scores given for neurologic deficits (Figure 2C). In addition propofol EDTA decreased the neurologic scores significantly at 7 days after MCAO (versus vehicle) (Figure 3B). Further, regional analysis revealed that treatment with propofol EDTA or propofol at 10 mins before ischemia reduced both infarct area and infarct volume in the cortex (Figure 4), although only propofol EDTA reduced infarct volume in the subcortex.

Histologic Observation of Cerebral Ischemic Damage

The morphologic features of TUNEL-stained cells (representing the ischemic damage and apoptotic cell death induced by 12 or 24 h MCAO) are shown in Figure 5. Cells exhibiting shrunken cell bodies and condensed nuclei were distributed in both the ischemic core and penumbra of the territory affected by MCAO, with the TUNEL-positive cells being among the population displaying such features. In this study, TUNEL-positive cells were predominantly located in the ischemic core region rather than in the ischemic penumbra, and propofol EDTA significantly reduced the number of TUNEL-positive cells in the ischemic penumbra (Figures 5C and 5D). We next distinguished apoptotic cells from necrotic cells, and each type was counted. Only densely labeled cells showing cell shrinkage, chromatin condensation, and fragmented nuclei indicating apoptosis were considered to be apoptotic cells, whereas cells with light diffus e labeling were taken as necrotic (Figure 5B). We compared only the numbers of apoptotic cells (yellow bar, Figures 5C and 5D). Propofol EDTA reduced this count significantly in the ischemic penumbra area at 24 h (but not 12 h) after MCAO.

EDTA Na Treatment

To examine whether EDTA Na might reduce infarct volume, we used TTC staining. Twenty-four hours after MCAO, mice had developed infarcts affecting the cortex and striatum. EDTA Na (0.5 mg/kg intravenously at 10 mins before MCAO) significantly reduced infarct volume, but brain swelling (edema) was not reduced (versus vehicle-treated mice) (Figures 6A and 6B). No significant changes were observed after administration of 0.05 mg/kg EDTA Na intravenously. Administration of 0.05 or 0.5 mg/kg EDTA Na did not reach to a significant level in the scores given for neurologic deficits significantly (Figure 6C).

Oxygen–Glucose Deprivation-Induced Apoptosis and Necrosis in PC12 Culture

Photographs of Hoechst 33342 and YO-PRO-1 staining are shown in Figure 7Aa to h. Hoechst 33342 stains all cells (live and dead cells), whereas YO-PRO-1 stains early-stage apoptotic and necrotic cells. Propofol or propofol plus EDTA (Figure 7Ag and h, respectively) decreased (versus vehicle treatment) the number of cells showing YO-PRO-1 staining after treatment with OGD. In a resazurin assay for the evaluation of cell viability, cell death was observed at 24 h after OGD treatment. Propofol inhibited OGD-induced cell death in a concentration-dependent manner (as evidenced by its effect on the increase in fluorescence intensity (λ_{ex} 560/λ_{em} 590 nm) associated with the reduction of resazurin to resorufin), its effect being significant at 20 μmol/L (Figure 7B). Similarly, EDTA significantly inhibited cell death at 0.05 μmol/L. Further, propofol plus EDTA inhibited cell death significantly more than propofol alone.

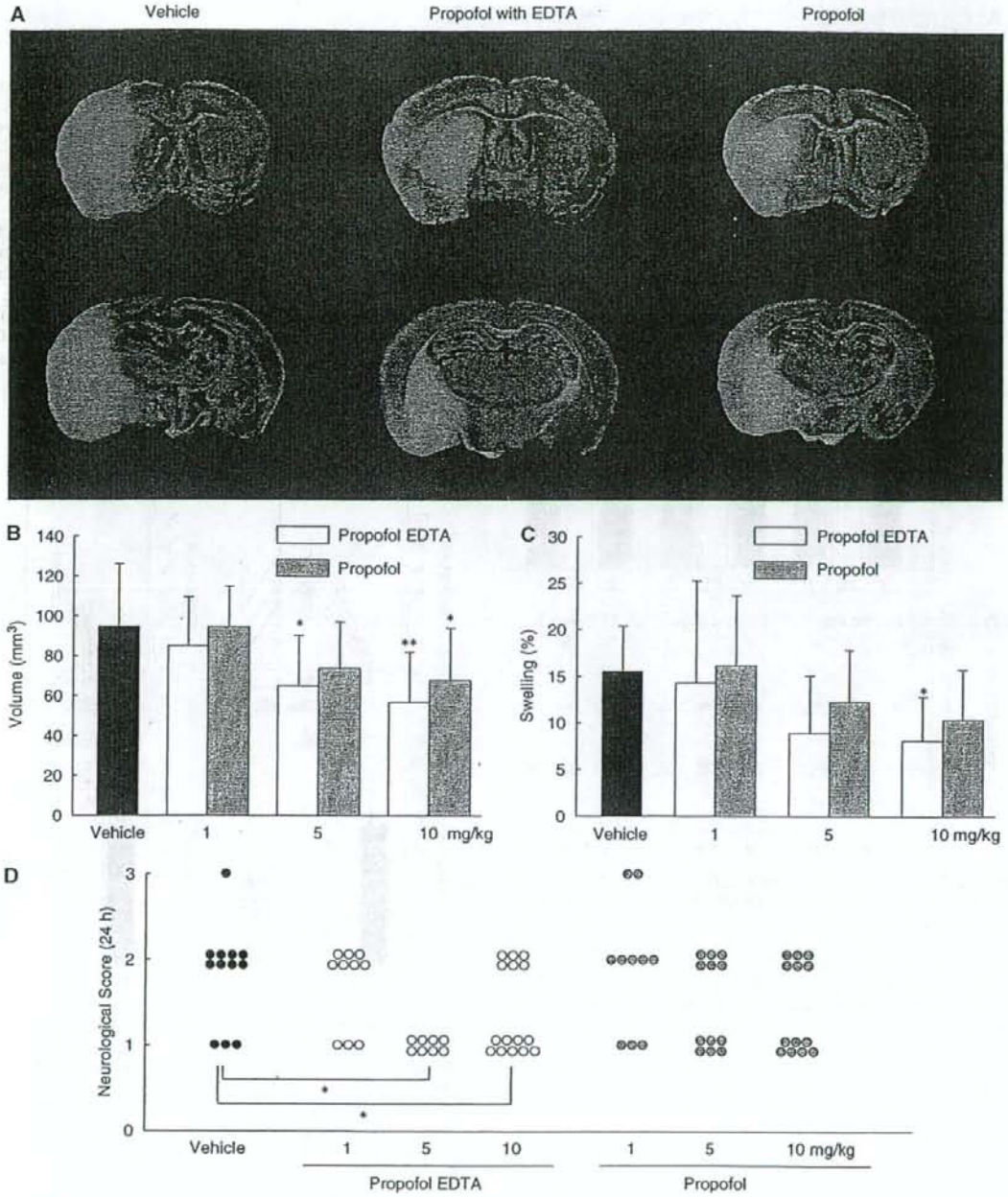

Figure 1 (**A**) 2,3,5-Triphenyltetrazolium chloride (TTC) staining of coronal brain sections (2 mm thickness) 24 h after permanent middle cerebral artery (MCA) occlusion in representative mice. Propofol or propofol EDTA (10 mg/kg intravenously) was administered 10 mins before the ischemia. Damaged tissue is shown as white areas. Sections on extreme left are from a vehicle-injected (control) mouse. Those in the center and on right are from mice administered propofol EDTA and propofol, respectively. (**B**) Effects of propofol EDTA and propofol on infarct volume at 24 h after permanent MCAO (each treatment being administered intravenously (1, 5, or 10 mg/kg, given over 90 secs, at 0.1 ml/10 g) 10 mins before MCAO). $^{*}P < 0.05$, $^{**}P < 0.01$ versus vehicle (Dunnett's test); $n = 10$ to 14. (**C**) The effects of propofol EDTA and propofol on brain swelling at 24 h after permanent MCAO in mice. $^{*}P < 0.05$ versus vehicle (Dunnett's test); $n = 10$ to 14. (**D**) Effects of propofol EDTA and propofol (details as in (**B**)) on neurologic deficits at 24 h after permanent MCAO. $^{*}P < 0.05$ versus vehicle (Mann–Whitney *U*-test); $n = 10$ to 14. Values are mean $\pm$ s.d.

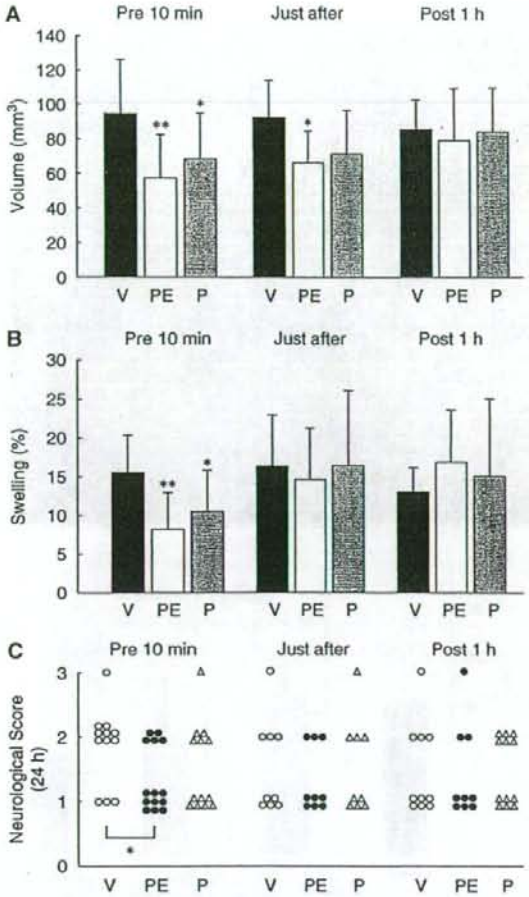

Figure 2 (**A**) Effects of propofol EDTA and propofol on infarct volume at 24 h after permanent MCAO (each treatment being administered intravenously (10 mg/kg) 10 mins before, after, or 1 h after the occlusion). Infarct areas in brain slices were stained with 2% TTC. $*P<0.05$, $**P<0.01$ versus vehicle (Dunnett's test); $n=9$ to 14. (**B**) Effects of propofol EDTA and propofol (details as in (**A**)) on brain swelling at 24 h after permanent MCAO. $*P<0.05$, $**P<0.01$ versus vehicle (Dunnett's test); $n=9$ to 14. (**C**) Effects of propofol EDTA and propofol (details as in (**A**)) on neurologic deficits at 24 h after permanent MCAO. $*P<0.05$ versus vehicle (Mann–Whitney U-test); $n=9$ to 14. Values are mean ± s.d.

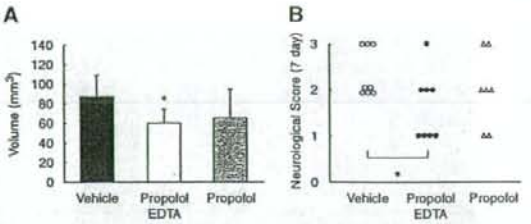

Figure 3 (**A**) Effects of propofol EDTA and propofol on infarct volume at 7 days after permanent MCAO (each treatment being administered intravenously (10 mg/kg) 10 mins before). $*P<0.05$ versus vehicle (Dunnett's test); $n=7$ to 8. (**B**) Effects of propofol EDTA and propofol (details as in (**A**)) on neurologic deficits at 7 days after permanent MCAO. $*P<0.05$ versus vehicle (Mann–Whitney U-test); $n=7$ to 8. Values are mean ± s.d.

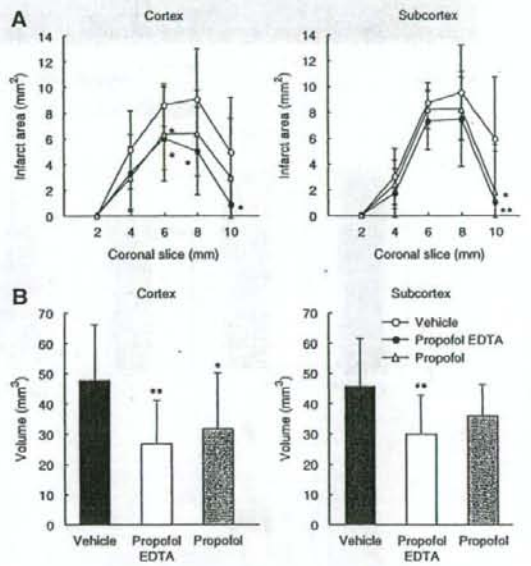

Figure 4 (**A**) Brain infarct areas (in cortex or subcortex) at 24 h after permanent middle cerebral artery (MCA) occlusion in mice. Propofol EDTA or propofol (each 10 mg/kg intravenously) was administered 10 mins before MCAO. $*P<0.05$, $**P<0.01$ versus vehicle (Dunnett's test); $n=12$ to 14. (**B**) Brain infarct volumes (in cortex or subcortex) at 24 h after permanent MCAO. $*P<0.05$, $**P<0.01$ versus vehicle (Dunnett's test); $n=12$ to 14. Values are mean ± s.d.

Measurement of Intracerebral Zinc Concentrations

Mice were assigned to four experiment groups (see Materials and methods). In the groups that did not undergo MCAO, no changes were found in the intracerebral zinc concentrations in vehicle-treated or propofol EDTA-treated mice. In the propofol EDTA-treated groups that underwent MCAO, the intracerebral zinc concentration in the cortex were decreased significantly (versus vehicle). Conversely, the intracerebral zinc concentration in the subcortical area slightly decreased, but it was not a significant change (versus vehicle). In vehicle-treated mice, there was no significant change in the intracerebral zinc concentrations by ischemia.

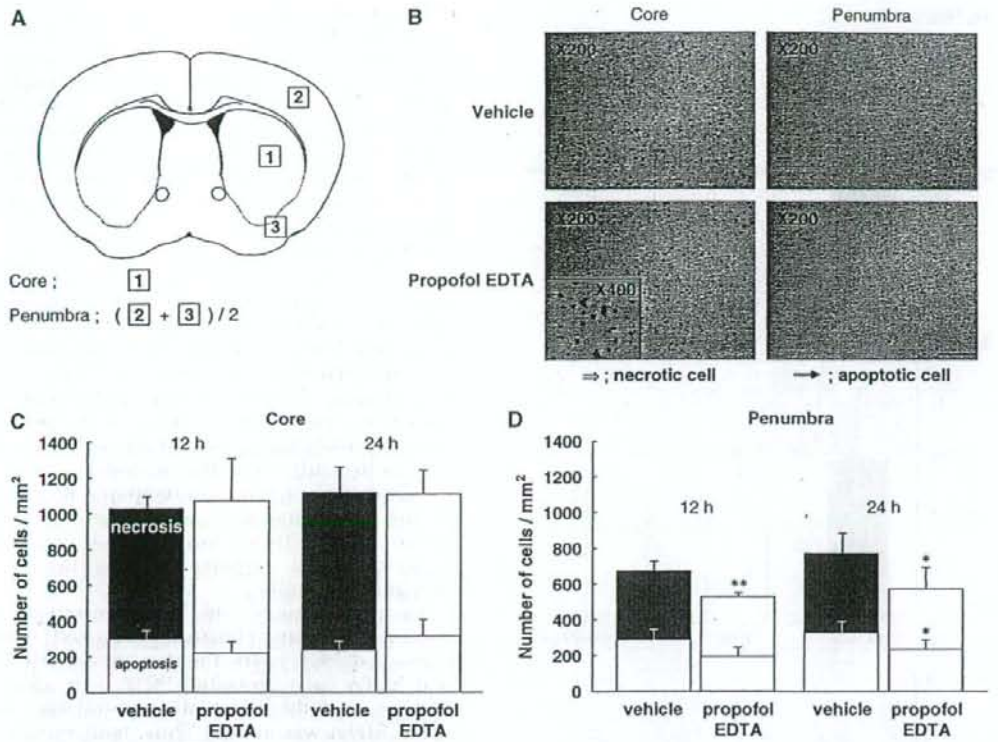

Figure 5 Effect of propofol EDTA on TUNEL staining after MCAO. Propofol EDTA (10 mg/kg intravenously) was administered 10 mins before MCAO, and mice were killed at 12 or 24 h after the occlusion. Terminal deoxynucleotidyl transferase-mediated dUTP nick end-labeling staining was performed as described in Materials and methods. **(A)** Schematic drawing showing the brain regions at a level of 0.4 to 1.0 mm anterior to bregma (through the anterior commissure). 1, ischemic core; 2 and 3, ischemic penumbra. The number of TUNEL-positive cells was counted in each of these areas, the average for areas 2 and 3 being taken as the number for the ischemic penumbra. **(B)** Propofol EDTA reduced the number of TUNEL-positive cells (versus vehicle treatment) in both the ischemic core and the ischemic penumbra. **(C and D)** Quantitative representation of TUNEL-positive cells in ischemic brains treated with propofol EDTA or vehicle. Yellow part of bar shows number of apoptotic cells among all positive cells. Note that a considerably smaller number of TUNEL-positive cells were observed at 24 h in the ischemic penumbra in mice treated with propofol EDTA than in mice treated with vehicle. However, in the ischemic core no such difference was detected. Data are expressed as mean ± s.d. $^{*}P < 0.05$, $^{**}P < 0.01$ versus vehicle (Student's *t*-test); $n = 4$ to 6. Scale bar = 100 μm.

Discussion

The main aim of this study was to compare the neuroprotective effects of propofol and propofol EDTA. The neuroprotective effects of propofol are well known, but to our knowledge little is known about neuroprotective effects of EDTA against ischemic damage. Because the chelating action of EDTA was a potential concern, we also examined the effect of propofol EDTA on intracerebral zinc homeostasis during focal cerebral ischemia.

For our *in vivo* study, we chose a permanent MCAO model because acute ischemic stroke in humans is frequently thromboembolic in nature and rarely undergoes spontaneous reperfusion. Both propofol (10 mg/kg, intravenously) and propofol EDTA (5 to 10 mg/kg, intravenously), when administered 10 mins before the occlusion, led (24 h later) to a smaller infarction, less brain swelling, and improvements in neurologic deficits (versus vehicle) (Figure 1B to 1D). A significant degree of protection was obtained when either drug was administered 10 mins before, but not 1 h after, MCAO (Figures 2A to 2C), with the propofol EDTA group apparently exhibiting the stronger neuroprotective effects. Furthermore, propofol EDTA (10 mg/kg, intravenously), when administered 10 mins before the occlusion, decreased infarct volume and the neurologic deficits significantly 7 days after MCAO (versus vehicle) (Figures 3A and 3B). Adembri *et al* (2006) reported that propofol reduced the size of the infarct and preserved spontaneous activity, even when its administration was delayed until up to 30 mins after permanent

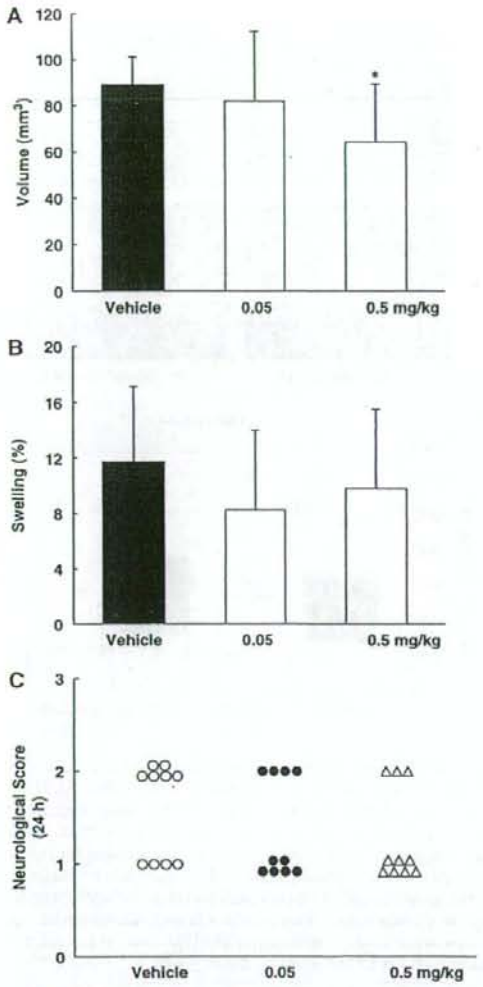

Figure 6 (**A**) Effects of EDTA Na on infarct volume at 24 h after permanent MCAO. $^*P < 0.05$ versus vehicle (Dunnett's test); $n = 10$. (**B**) Effects of EDTA Na on brain swelling at 24 h after permanent MCAO in mice (Dunnett's test) ($n = 10$). (**C**) Effects of EDTA Na on neurologic deficits at 24 h after permanent MCAO (Mann–Whitney *U*-test) ($n = 10$). Values are mean ± s.d.

MCAO in rats. In our study, on a different species (mice), only propofol EDTA (not propofol) administration after MCAO reduced the infarct volume significantly, and it did not reduce either the brain swelling or the scores given for neurologic deficits. Moreover, when propofol and propofol EDTA were administered 1 h after MCAO, neither displayed any neuroprotective effects. However, as propofol and propofol EDTA are widely used as anesthetic agents in many surgical procedures and as sedatives for intensive care patients, they will already be present if cerebral ischemia develops during an operation or sedation, and might then provide a valuable neuroprotective effect. However, we have to mention that, in this study, propofol and propofol EDTA protected neurons against ischemia-induced neuronal damage under a hyperglycemic condition (see Table 1). Brown *et al* (2005) have reported that anesthesia can cause sustained hyperglycemia. The anesthesia or the operation might increase the blood glucose level, presumably by the secreted catecholamine during an operation by ache irritation.

Ischemia-induced TUNEL-positive cells were found in both the ischemic penumbra and core regions in control mice, and propofol EDTA significantly reduced their number in the ischemic penumbra (Figures 5C and 5D). Terminal deoxynucleotidyl transferase-mediated dUTP nick end-labeling staining detects nuclear DNA fragmentation, which has been reported to occur in both necrosis and apoptosis. Indeed, we observed TUNEL-positive morphologically necrotic neurons mainly in the ischemic core, in addition to apoptotic ones mainly in the inner boundary zone of the infarct (Kitagawa *et al*, 1998). Thus, our research suggests that propofol EDTA inhibits apoptosis mainly in the ischemic penumbra.

Next, we examined the *in vitro* effects of propofol and EDTA against OGD-induced cell damage in cultures of PC12 cells (Figures 7A and 7B). Propofol and EDTA each protected PC12 cells against such damage, and the effect of propofol was enhanced when EDTA was added. Thus, both *in vitro* and *in vivo*, propofol plus EDTA had a stronger neuroprotective effect than propofol alone. These findings indicate that the protective effects of propofol on ischemic damage are in part due to a neuron-direct mechanism. We therefore examined the neuroprotective effect of EDTA administered alone, and we found that EDTA Na (0.5 mg/kg intravenously) significantly reduced only the infarct volume. Because 0.005% disodium edetate (EDTA) is included in the generally used preparation of propofol EDTA, 10 mg/kg propofol EDTA has 0.05 mg/kg EDTA. A significant neuroprotection was seen with that level of EDTA when 10 times that concentration (0.05 mg/kg) was used. For EDTA to pass from blood into brain tissue, it must cross either the blood–brain barrier or the blood–cerebrospinal fluid barrier; it is well known that EDTA can hardly cross the blood–brain barrier (Fenstermacher and Kaye, 1998). However, the oxidative stress generated during stroke can lead to blood–brain barrier disruption, with secondary vasogenic edema and hemorrhagic transformation of infarcted brain tissue, so that enough EDTA may cross the blood–brain barrier at times of cerebral ischemia to exert neuroprotective effects.

EDTA is a potent chelator of heavy metals such as zinc, iron, copper, manganese, chromium, cobalt, and lead (Herr *et al*, 2000). We focused on zinc as it is one of the most abundant transition metals in the brain, and is essential for development, growth,

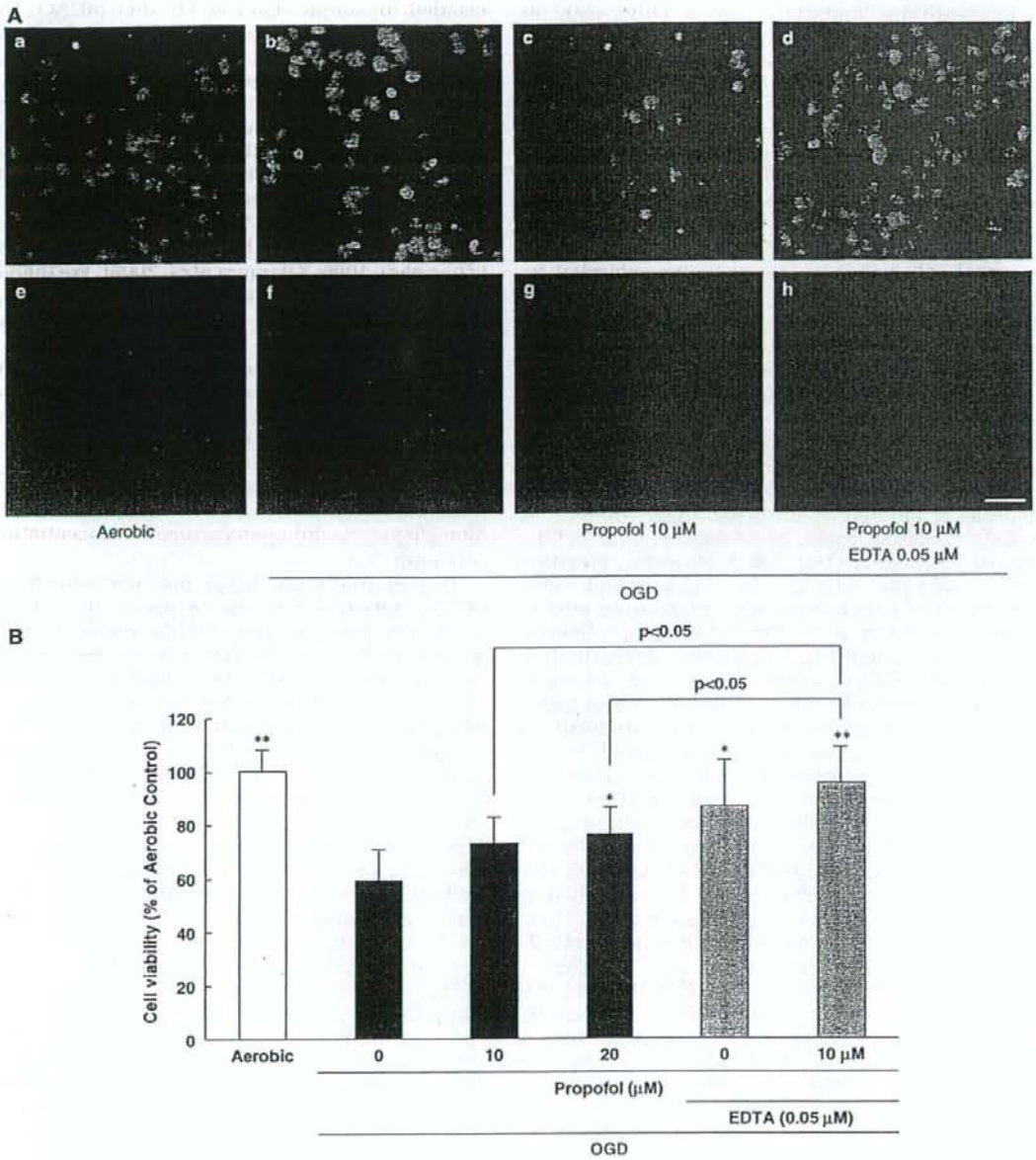

Figure 7 (**A**) Representative fluorescence microscopy of Hoechst 33342 (blue) and YO-PRO-1 (green) staining at 24 h after oxygen–glucose deprivation (OGD). (a and e): (a) nontreated cells showed normal nuclear morphology and (e) were negative for YO-PRO-1 (early-stage apoptotic and necrotic cells are YO-PRO-1-positive). (b and f): (b) OGD-induced neurotoxicity, with cells showing condensation and fragmentation of their nuclei, including YO-PRO-1-positively stained cells (f). (c and g) and (d and h): (c) Pretreatment with 10 μmol/L propofol or 10 μmol/L propofol plus 0.05 μmol/L EDTA reduced both the nuclear condensation (c and d, respectively) and YO-PRO-1-positive staining (g and h, respectively) induced by OGD treatment. (a and e): control; (b and f): vehicle-treatment plus OGD; (c and g): propofol 10 μmol/L plus OGD; (d and h): propofol 10 μmol/L and EDTA 0.05 μmol/L plus OGD; (a to d): Hoechst 33342 staining; (e to h): YO-PRO-1 staining. Scale bar = 40 μm. (**B**) Both propofol and propofol EDTA reduced the cell damage induced by OGD in PC12 culture. Cell viability was assessed after immersion in 10% resazurin solution for 3 h at 37°C, and fluorescence was recorded at 560/590 nm. OGD-induced cell death, and propofol and EDTA each inhibited this OGD-induced cell death. Propofol plus EDTA reduced cell death by more than propofol alone. Data are expressed as mean$\pm$s.d. $^{*}P < 0.05$, $^{**}P < 0.01$ versus OGD treatment alone (Dunnett's test or Student's *t*-test); $n = 4$.